 CMC, vol.41, no.2, pp.111-152, 2014

Exact Solutions for the Stability and Free Vibration of Multilayered Functionally Graded Material Hollow Cylinders under Axial Compression

Chih-Ping Wu[1,2], **Ruei-Yong Jiang**[1] **and Sheng-Yao Tu**[1]

Abstract: Exact three-dimensional stability and free vibration analyses of simply-supported, multilayered functionally graded material (FGM) circular hollow cylinders and laminated composite ones under axial compression are presented. The material properties of each FGM layer are assumed to obey a power-law distribution of the volume fractions of constituents through the thickness coordinate. The Pagano method, which is based on the principle of virtual displacement and is conventionally used for the analysis of laminated composite structures, is modified to be feasible for the study of multilayered FGM cylinders, in which Reissner's mixed variational theorem, the successive approximation and transfer matrix methods, and the transformed real-valued solutions of the system equations are used. The present modified Pagano solutions for laminated composite cylinders are in excellent agreement with the exact 3D ones available in the literature, and those for sandwich FGM cylinders may be used as the benchmark solutions to assess the ones obtained using various two-dimensional theories and numerical models. The influence of some effects on the lowest critical load parameters of multilayered FGM cylinders and laminated composite ones is investigated, such as the derivation between using von Karman nonlinearity and full kinematic one, and the difference between using the uniform stress assumption and the uniform strain one. In addition, a parametric study with regard to some effects on the lowest frequency parameters of axially loaded, multilayered FGM cylinders is carried out, such as the magnitude of the applied compressive loads, the radius-to-thickness, length-to-radius and orthotropic ratios, and the material-property gradient index.

Keywords: Elasticity, Reissner's mixed variational theorem, Vibration, Buckling, Functionally graded materials, Cylinders.

[1] Department of Civil Engineering, National Cheng Kung University, Tainan 70101, Taiwan, ROC.
[2] Corresponding author. Fax: +886-6-2370804; Email: cpwu@mail.ncku.edu.tw

1 Introduction

It is well-known that the laminated fiber-reinforced composite material (FRCM) structures have a mismatch of material properties across the interfaces between adjacent layers, and this may result in some drawbacks, such as delamination, matrix cracking, and local buckling occurring at these locations, especially when they operate in high temperature environments. To overcome these disadvantages, an emerging class of functionally graded material (FGM) structures, the material properties of which are heterogeneous and gradually and continuously vary through the thickness coordinate, has been developed. The feature of continuous distributions of material properties through the thickness coordinate of FGM structures, however, also increases the complexity and difficulty of analyzing such structures.

The conventional two-dimensional (2D) first- and higher-order shear deformation theories (FSDT and HSDT) have been successfully extended to the related stability and free vibration analyses of functionally grade (FG) elastic/piezoelectric plates and shells. Based on the classical plate theory (CPT), FSDT and HSDT, Chen et al. (2008), Chen (2005), Chen et al. (2006, 2009) investigated the stability and free vibration of functionally graded plates, in which the corresponding governing equations for the FGM plates subjected to a general state of non-uniform initial stress were derived, the material properties of the FGM plates were assumed to obey a simple power law of volume fractions of constituents varying through the thickness direction, and the effects of various parameters and initial stresses on the lowest critical load and frequency parameters of the FGM plates were examined. Najafov et al. (2013) presented the torsional vibration and stability of FGM cylindrical shells on elastic foundations using the classical shell theory. Matsunaga (2007, 2008, 2009) developed a 2D HSDT to examine the stability and free vibration problems of FGM circular cylindrical shells, in which a set of governing equations accounting for the effects of transverse shear and normal deformations were derived using Hamilton's principle, and the material properties were assumed to vary according to a power law distribution in terms of the volume fractions of the constituents. Based on the FSDT, Sheng and Wang (2008, 2010) analyzed the thermoelastic vibration and buckling problems of functionally graded piezoelectric (or elastic) cylindrical shells embedded and not embedded in an elastic medium, in which the effects of the material-property gradient index and shell geometry parameters on the critical loads, temperature increments, and voltages were presented.

Some advanced finite element methods (FEMs) have been developed for the analysis of FGM structures. Dong and Atluri (2011) presented a simple procedure to formulate efficient and stable hybrid/mixed elements for various engineering applications in macro- and micro-mechanics. Implementations of these FEMs, it is demonstrated that they are numerically stable, and are more efficient than tradi-

tional hybrid/mixed elements. Subsequently, following the procedure, Dong et al. (2014) developed a simple four-node locking-alleviated mixed FEM for the analysis of FGM composite beams, in which there are no needs to assume the higher-order or layerwise zig-zag displacement variations through the thickness coordinate in advance, which were commonly used for the displacement-based FEMs in the literature.

Wu et al. (2008) classified the exact three-dimensional (3D) analytical approaches for multilayered FRCM plates and shells into four different ones, namely the Pagano (1969, 1970), state space, series expansion, and perturbation ones, in which the pioneering studies that initiated the development of various approaches and their relevant applications were summarized, comparisons among the results obtained using various approaches were carried out, and applications of these to assorted 3D analyses of laminated FRCM structures were collected and tabulated. Among these, it is apparent that the Pagano method, based on the principle of virtual displacement (PVD), is both simple and the most widely applied for laminated FRCM structures, while it is not feasible for their FGM counterparts without further modifications even though other approaches have been successfully applied to the analysis of FGM structures, such as the use of the state space approach (Chen and Ding, 2002; Chen and Wang, 2002; Chen et al., 2004; Wu and Liu, 2007) and perturbation one (Wu and Tsai, 2004, 2009, 2010; Wu and Syu, 2007).

In order to achieve the above-mentioned purpose, Wu et al. (2010) and Wu and Lu (2009) developed a modified Pagano method for the exact 3D static and free vibration analyses of simply supported, functionally graded magneto-electro-elastic plates, and it was further extended to the bending and thermo-elastic analyses of functionally graded piezoelectric sandwich cylinders by Wu and Tsai (2011) and Wu and Jiang (2011). The modifications to the original Pagano method are as follows: (a) The Reissner mixed variational theorem- (RMVT)-based formulation (Reissner, 1984, 1986), rather than the PVD-based one, is used so that both the lateral boundary conditions on the outer surfaces and the continuity conditions at the interface between adjacent layers can be directly applied. (b) The sets of complex-valued solutions for system equations are transferred to the corresponding sets of real-valued solutions by means of Euler's formula for the purpose of computational efficiency. (c) A successive approximation (SA) method is adopted, in which the functionally graded plate or shell considered is artificially divided into a certain number of individual layers with an equal and small thickness, as compared to the in-plane dimensions of the plate or the mid-surface radius of the shell for each layer. Using this refinement, one may reasonably approximate the variable material coefficients of each layer to the constant material coefficients in an average thickness sense so that the system of thickness-varying differential equations for

each individual layer can be reduced to a system of thickness-invariant differential ones. (d) A transfer matrix method is developed, so that the general solutions of system equations can be obtained layer-by-layer and the related computation is not time-consuming.

The stability and free vibration problems of isotropic, FRCM and FGM circular hollow cylinders have attracted much attention for several decades because stability is the dominant failure occurring in these structures, and free vibration is the basic characteristic required for the design work, while relatively few 3D stability and free vibration analyses of axially loaded, multilayered FGM cylinders can be found in the open literature in comparison with 2D and 3D analyses of laminated FRCM structures, and the 2D analysis of FGM ones. Due to the benefits of the modified Pagano method, as noted above, it is extensively applied in this article to the exact 3D stability and free vibration analyses of simply-supported, multilayered FGM/FRCM circular hollow cylinders under axial compression, in which the material properties of each FGM layer are assumed to obey a power-law distribution of the volume fractions of the constituents varying through the thickness coordinate, and the magnitude of the applied compressive load is less than the lowest critical load of the cylinder, which is obtained using 3D linear buckling theory with an assumed 3D displacement field for the pre-buckling state of the cylinder. Because the FGM cylinder is transformed into a multilayered homogeneous elastic one in this formulation using the SA method, the analysis of multilayered (or sandwiched) FRCM cylinders can thus be included as a special case, and be undertaken using the present formulation. A parametric study is thus carried out of the influence of the radius-to-thickness, length-to-radius, orthotropic ratios, and the material-property gradient index on the lowest critical load and frequency parameters of simply-supported, laminated FGM/FRCM cylinders under axial compression.

2 Prebuckling state in a multilayered FGM cylinder

We consider a simply supported, multilayered functionally graded orthotropic circular hollow cylinder under an axial compressive load with the magnitude P_x, as shown in Fig. 1(a). A global cylindrical coordinate system (x, θ and r coordinates) is adopted and located at the center of the cylinder, and a global thickness coordinate (ζ) and a set of local thickness coordinates (z_m , $m = 1, 2, \cdots, N_l$) are located at the middle surfaces of the cylinder and each individual layer, respectively, as shown in Fig. 1(b), where N_l denotes the total number of layers constituting the cylinder. The thicknesses of each individual layer and the cylinder are h_m $(m = 1, 2, \cdots, N_l)$ and H, respectively, while $\sum_{m=1}^{N_l} h_m = H$, and R and L denote the mid-surface radius and length of the cylinder. The relationship between

the radial coordinate and the global thickness coordinate is $r = R + \zeta$, and that between the global and local thickness coordinates in the m^{th}-layer is $\zeta = \bar{\zeta}_m + z_m$, in which $\bar{\zeta}_m = (\zeta_m + \zeta_{m-1})/2$, and ζ_m and ζ_{m-1} are the global thickness coordinates measured from the middle surface of the cylinder to the top and bottom surfaces of the m^{th}-layer, respectively.

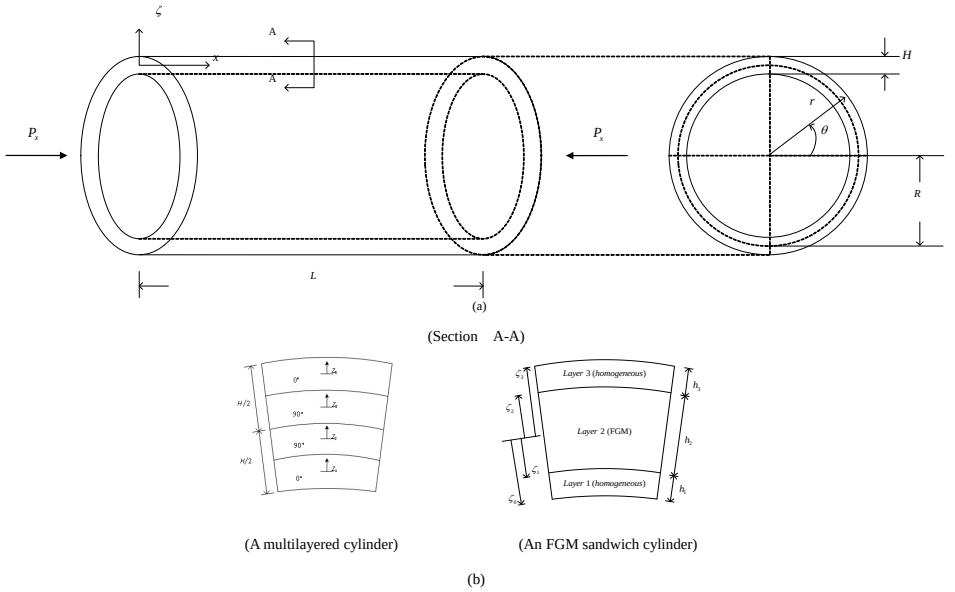

Figure 1: (a) The configuration and dimensions of an FGM sandwich cylinder or a laminated composite one, (b) the local and global coordinates of the cylinder.

According to the assumptions of linear stability theory, a set of normal stresses exists in the cylinder just before instability occurs when the cylinder is subjected to an axial compressive load, in which the displacement components of the m^{th}-layer at the initial position are expected in the following form, which are given by slightly modifying the ones in Ye and Soldatos (1995) and Soldatos and Ye (1994),

$$\bar{u}_x^{(m)} = A_0 x, \quad m = 1, 2, \cdots, N_l \tag{1a}$$

$$\bar{u}_\theta^{(m)} = 0, \quad m = 1, 2, \cdots, N_l \tag{1b}$$

$$\bar{u}_r^{(m)} = A_0 \, \bar{W}_0^{(m)}(\zeta) \quad m = 1, 2, \cdots, N_l, \tag{1c}$$

where A_0 denotes a uniform normal strain produced in the axial direction, which is an arbitrary constant and can be determined later in this work by means of satisfying the force equilibrium equation in the axial direction at the edges.

According to the initial displacement model given in Eq. (1), it is assumed that in the pre-buckling state the cylinder is free of initial shear stresses (i.e., $\bar{\tau}_{xr}^{(m)} = \bar{\tau}_{\theta r}^{(m)} = \bar{\tau}_{x\theta}^{(m)} = 0$, $m = 1, 2, \cdots, N_l$), and the initial normal stresses in the m^{th}-layer can be expressed as

$$\bar{\sigma}_x^{(m)}(\zeta) = A_0\, \bar{\sigma}_{x0}^{(m)}(\zeta), \quad m = 1, 2, \cdots, N_l \tag{2a}$$

$$\bar{\sigma}_\theta^{(m)}(\zeta) = A_0\, \bar{\sigma}_{\theta 0}^{(m)}(\zeta), \quad m = 1, 2, \cdots, N_l \tag{2b}$$

$$\bar{\sigma}_r^{(m)}(\zeta) = A_0\, \bar{\sigma}_{r0}^{(m)}(\zeta), \quad m = 1, 2, \cdots, N_l \tag{2c}$$

where $\bar{\sigma}_{x0}^{(m)} = Q_{11}^{(m)} + \left(Q_{12}^{(m)}/r\right) \bar{W}_0^{(m)} + Q_{13}^{(m)}\, \bar{\sigma}_{r0}^{(m)}$,

$\bar{\sigma}_{\theta 0}^{(m)} = Q_{12}^{(m)} + \left(Q_{22}^{(m)}/r\right) \bar{W}_0^{(m)} + Q_{23}^{(m)}\, \bar{\sigma}_{r0}^{(m)}$,

$\bar{\sigma}_{r0}^{(m)} = c_{13}^{(m)} + \left(c_{23}^{(m)}/r\right) \bar{W}_0^{(m)} + c_{33}^{(m)} \left(\bar{W}_0^{(m)},_\zeta\right)$,

$Q_{ij}^{(m)} = c_{ij}^{(m)} - \left(c_{i3}^{(m)}\, c_{j3}^{(m)}/c_{33}^{(m)}\right) \quad (i,\ j = 1,\ 2 \text{ and } 6)$,

$Q_{k3}^{(m)} = c_{k3}^{(m)}/c_{33}^{(m)} \quad (k = 1 \text{ and } 2)$,

and $c_{ij}^{(m)}$ denotes the material elastic coefficients of the m^{th}-layer, which is a constant for the multilayered composite cylinder and a function of the thickness coordinate for the multilayered FGM one, and the comma denotes partial differentiation with respect to the suffix variable.

According to the initial displacement model given in Eq. (1), the stress equilibrium equations in the axial and circumferential directions are automatically satisfied, and the one in the radial (or thickness) direction is given as follows:

$$\bar{\sigma}_{r0}^{(m)},_\zeta = \left[\left(Q_{23}^{(m)} - 1\right)/r\right] \bar{\sigma}_{r0}^{(m)} + \left(Q_{22}^{(m)}/r^2\right) \bar{W}_0^{(m)} + \left(Q_{12}^{(m)}/r\right). \tag{3}$$

Using Eqs. (2c) and (3), we can write the state space equations of the pre-buckling state of the cylinder in the following form

$$\frac{d\,\bar{\mathbf{F}}^{(m)}}{d\,\zeta} = \bar{\mathbf{K}}^{(m)}\, \bar{\mathbf{F}}^{(m)} + \bar{\mathbf{K}}_p^{(m)}, \tag{4}$$

where

$$\bar{\mathbf{F}}^{(m)} = \begin{Bmatrix} \bar{W}_0^{(m)}(\zeta) \\ \bar{\sigma}_{r0}^{(m)}(\zeta) \end{Bmatrix}, \bar{\mathbf{K}}^{(m)} = \begin{bmatrix} \bar{k}_{11}^{(m)} & \bar{k}_{12}^{(m)} \\ \bar{k}_{21}^{(m)} & \bar{k}_{22}^{(m)} \end{bmatrix}, \bar{\mathbf{K}}_p^{(m)} = \begin{Bmatrix} -Q_{13}^{(m)} \\ \left(Q_{12}^{(m)}/r\right) \end{Bmatrix},$$

$$\bar{k}_{11}^{(m)} = -Q_{23}^{(m)}/r,\ \bar{k}_{12}^{(m)} = \left(1/c_{33}^{(m)}\right),\ \bar{k}_{21}^{(m)} = \left(Q_{22}^{(m)}/r^2\right) \text{ and } \bar{k}_{22}^{(m)} = \left(Q_{23}^{(m)} - 1\right)/r.$$

By means of the traction conditions imposed on the lateral surfaces of the cylinder, we can readily solve Eq. (4) using the transfer matrix method combined with an SA method, the solution procedure of which is described in Wu and Jiang (2007) and not repeated here, and then the initial normal stresses can be subsequently obtained.

In the cases of pure axial compression, the traction conditions on the lateral surfaces are

$$\bar{\sigma}_r^{(N_l)}(\zeta = H/2) = 0 \quad \text{and} \quad \bar{\sigma}_r^{(1)}(\zeta = -H/2) = 0. \tag{5}$$

As mentioned above, the functions of $\bar{W}_0^{(m)}(\zeta)$ and $\bar{\sigma}_{r0}^{(m)}(\zeta)$ can be determined using the transfer matrix method combined with the SA one.

Taking a free body diagram at each edge, we can express the force equilibrium equation in the axial direction as follows:

$$\int_0^{2\pi} \int_{\zeta_0}^{\zeta_{N_l}} \bar{\sigma}_x(\zeta)\ r\, d\zeta\, d\theta = -P_x. \tag{6}$$

By satisfying Eq. (6), we subsequently obtain the expression of A_0, as follows:

$$A_0 = -S_x P_x, \tag{7}$$

in which

$$S_x = \left\{ 2\pi R \sum_{m=1}^{N_l} \int_{\zeta_{m-1}}^{\zeta_m} \left[Q_{11}^{(m)} + \left(Q_{12}^{(m)}/r\right) \bar{W}_0^{(m)} + Q_{13}^{(m)}\, \bar{\sigma}_{r0}^{(m)} \right] [1 + (\zeta/R)]\, d\zeta \right\}^{-1}.$$

As a result, the initial normal stresses can be obtained:

$$\bar{\sigma}_x^{(m)}(\zeta) = -f_x^{(m)}(\zeta)\, P_x,\ \bar{\sigma}_\theta^{(m)}(\zeta) = -f_\theta^{(m)}(\zeta)\, P_x,\ \text{and}\ \bar{\sigma}_r^{(m)}(\zeta) = -f_r^{(m)}(\zeta)\, P_x, \tag{8}$$

in which $f_x^{(m)}$, $f_\theta^{(m)}$ and $f_r^{(m)}$ denote the influence functions of the initial normal stresses for the m^{th}-layer of the cylinder in the cases of pure axial compression, and $f_x^{(m)} = S_x \left[Q_{11}^{(m)} + \left(Q_{12}^{(m)}/r\right) \bar{W}_0^{(m)} + Q_{13}^{(m)}\, \bar{\sigma}_{r0}^{(m)} \right]$, $f_\theta^{(m)} = S_x \left[Q_{12}^{(m)} + \left(Q_{22}^{(m)}/r\right) \bar{W}_0^{(m)} + Q_{23}^{(m)}\, \bar{\sigma}_{r0}^{(m)} \right]$, and $f_r^{(m)} = S_x\, \bar{\sigma}_{r0}^{(m)}$, while their dimensionless counterparts are $\hat{f}_k^{(m)} = f_k^{(m)}(2\pi RH)$, $(k = x, \theta, r)$.

3 RMVT-based Hamilton principle

3.1 RMVT-based Lagrangian functional

As above-mentioned, a set of initial state of normal stresses given in Eq. (8) exists in the cylinder just before instability occurs, and is introduced in the RMVT-based Lagrangian functional (L_R) of an initially stressed, multilayered FGM cylinder later in this work.

The stress-strain relations valid for the nature of the symmetry class of elastic materials are given by

$$\begin{Bmatrix} \sigma_x^{(m)} \\ \sigma_\theta^{(m)} \\ \sigma_r^{(m)} \\ \tau_{\theta r}^{(m)} \\ \tau_{xr}^{(m)} \\ \tau_{x\theta}^{(m)} \end{Bmatrix} = \begin{bmatrix} c_{11}^{(m)} & c_{12}^{(m)} & c_{13}^{(m)} & 0 & 0 & 0 \\ c_{12}^{(m)} & c_{22}^{(m)} & c_{23}^{(m)} & 0 & 0 & 0 \\ c_{13}^{(m)} & c_{23}^{(m)} & c_{33}^{(m)} & 0 & 0 & 0 \\ 0 & 0 & 0 & c_{44}^{(m)} & 0 & 0 \\ 0 & 0 & 0 & 0 & c_{55}^{(m)} & 0 \\ 0 & 0 & 0 & 0 & 0 & c_{66}^{(m)} \end{bmatrix} \begin{Bmatrix} \varepsilon_x^{(m)} \\ \varepsilon_\theta^{(m)} \\ \varepsilon_r^{(m)} \\ \gamma_{\theta r}^{(m)} \\ \gamma_{xr}^{(m)} \\ \gamma_{x\theta}^{(m)} \end{Bmatrix}, \tag{9}$$

where $\sigma_x^{(m)}$, $\sigma_\theta^{(m)}$, $\cdots$, $\tau_{x\theta}^{(m)}$ and $\varepsilon_x^{(m)}$, $\varepsilon_\theta^{(m)}$, $\cdots$, $\gamma_{x\theta}^{(m)}$ are the stress and strain components of a certain material point in the m^{th}-layer, respectively; $c_{ij}^{(m)}$ (i, j=1–6) are the elastic coefficients which are constants through the thickness coordinate in the homogeneous elastic layers, and are variable through the thickness coordinate in the FGM layers (i.e., $c_{ij}^{(m)}(\zeta)$ or $c_{ij}^{(m)}(z_m)$).

The kinematic relations between the strainsand displacements are given by

$$\begin{Bmatrix} \varepsilon_x^{(m)} \\ \varepsilon_\theta^{(m)} \\ \varepsilon_r^{(m)} \\ \gamma_{\theta r}^{(m)} \\ \gamma_{xr}^{(m)} \\ \gamma_{x\theta}^{(m)} \end{Bmatrix} = \begin{bmatrix} \partial_x & 0 & 0 \\ 0 & (1/r)\,\partial_\theta & (1/r) \\ 0 & 0 & \partial_r \\ 0 & (-1/r)+\partial_r & (1/r)\,\partial_\theta \\ \partial_r & 0 & \partial_x \\ (1/r)\,\partial_\theta & \partial_x & 0 \end{bmatrix} \begin{Bmatrix} u_x^{(m)} \\ u_\theta^{(m)} \\ u_r^{(m)} \end{Bmatrix}, \tag{10}$$

where $u_x^{(m)}$, $u_\theta^{(m)}$ and $u_r^{(m)}$ denote the elastic displacement components, $\partial_k = \partial/\partial k \quad (k = x,\ \theta \text{ and } r)$.

The RMVT-based Lagrangian functional of the FGM cylinder under axial compression is written in the form of

$$L_R = T_R - \Pi_R, \tag{11}$$

in which T_R and Π_R denote the kinetic and RMVT-based potential energy functions, and are given as

$$T_R = (1/2)\sum_{m=1}^{N_l}\int_{-h_m/2}^{h_m/2}\int_{\Omega}\rho^{(m)}\left[\left(\partial u_x^{(m)}/\partial t\right)^2+\left(\partial u_\theta^{(m)}/\partial t\right)^2+\left(\partial u_r^{(m)}/\partial t\right)^2\right]r dx d\theta dz_m, \tag{12}$$

$$\begin{aligned}\Pi_R = &\sum_{m=1}^{N_l}\int_{-h_m/2}^{h_m/2}\int_{\Omega}\left[\sigma_x^{(m)}\varepsilon_x^{(m)}+\sigma_\theta^{(m)}\varepsilon_\theta^{(m)}+\sigma_r^{(m)}\varepsilon_r^{(m)}+\tau_{xr}^{(m)}\gamma_{xr}^{(m)}+\tau_{\theta r}^{(m)}\gamma_{\theta r}^{(m)}+\tau_{x\theta}^{(m)}\gamma_{x\theta}^{(m)}-B(\sigma_{ij}^{(m)})\right]r dx d\theta dz_m\\ &+\sum_{m=1}^{N_l}\int_{-h_m/2}^{h_m/2}\int_{\Omega}\left[\left(\bar{\sigma}_x^{(m)}\right)\left(\hat{\varepsilon}_x^{(m)}\right)+\left(\bar{\sigma}_\theta^{(m)}\right)\left(\hat{\varepsilon}_\theta^{(m)}\right)+\left(\bar{\sigma}_r^{(m)}\right)\left(\hat{\varepsilon}_r^{(m)}\right)\right]r dx d\theta dz_m\\ &-\sum_{m=1}^{N_l}\int_{-h_m/2}^{h_m/2}\int_{\Gamma_\sigma}\bar{T}_i^{(m)}u_i^{(m)}d\Gamma dz_m-\sum_{m=1}^{N_l}\int_{-h_m/2}^{h_m/2}\int_{\Gamma_u}T_i^{(m)}(u_i^{(m)}-\bar{u}_i^{(m)})d\Gamma dz_m\end{aligned}, \tag{13}$$

in which $\rho^{(m)}$ and t stand for the mass density of the m^{th}-layer and the time variable, respectively; Ω denotes the cylinder domain on the $x-\theta$ surface; Γ_σ and Γ_u are the portions of the edge boundary, where the surface tractions $\bar{T}_i^{(m)}$ ($i = x,\ \theta$ and r) and surface displacements $\bar{u}_i^{(m)}$ ($i = x,\ \theta$ and r) are prescribed, respectively; $B(\sigma_{ij}^{(m)})$ is the complementary energy density function; $\hat{\varepsilon}_x^{(m)}$, $\hat{\varepsilon}_\theta^{(m)}$ and $\hat{\varepsilon}_r^{(m)}$ denote the second-order terms of the Green-Lagrange normal strains, and are given by

$$\hat{\varepsilon}_x^{(m)} = (1/2)\left[\left(u_x^{(m)},_x\right)^2+\left(u_\theta^{(m)},_x\right)^2+\left(u_r^{(m)},_x\right)^2\right], \tag{14a}$$

$$\hat{\varepsilon}_\theta^{(m)} = \left(1/2r^2\right)\left[\left(u_x^{(m)},_\theta\right)^2+\left(u_\theta^{(m)},_\theta+u_r\right)^2+\left(u_r^{(m)},_\theta-u_\theta\right)^2\right], \tag{14b}$$

$$\hat{\varepsilon}_r^{(m)} = (1/2)\left[\left(u_x^{(m)},_r\right)^2+\left(u_\theta^{(m)},_r\right)^2+\left(u_r^{(m)},_r\right)^2\right]. \tag{14c}$$

In this RMVT-based formulation, we take the elastic displacement and transverse stress components as primary variables subject to variation, and the in- and out-of-surface strain and in-surface stress components are dependent variables, which can be expressed in terms of primary variables using Eqs. (1)–(2) as follows:

$$\varepsilon_x^{(m)} = \partial B/\partial\sigma_x^{(m)} = u_x^{(m)},_x, \tag{15}$$

$$\varepsilon_\theta^{(m)} = \partial B/\partial\sigma_\theta^{(m)} = (1/r)\,u_\theta^{(m)},_\theta+(1/r)\,u_r^{(m)}, \tag{16}$$

$$\varepsilon_r^{(m)} = \partial B/\partial \sigma_r^{(m)} = -Q_{13}^{(m)} u_x^{(m)},_x - \left(Q_{23}^{(m)}/r\right) u_\theta^{(m)},_\theta - \left(Q_{23}^{(m)}/r\right) u_r^{(m)} + \left(1/c_{33}^{(m)}\right) \sigma_r^{(m)}, \tag{17}$$

$$\gamma_{xr}^{(m)} = \partial B/\partial \tau_{xr}^{(m)} = \left(1/c_{55}^{(m)}\right) \tau_{xr}^{(m)}, \tag{18}$$

$$\gamma_{\theta r}^{(m)} = \partial B/\partial \tau_{\theta r}^{(m)} = \left(1/c_{44}^{(m)}\right) \tau_{\theta r}^{(m)}, \tag{19}$$

$$\gamma_{x\theta}^{(m)} = \partial B/\partial \tau_{x\theta}^{(m)} = (1/r)\, u_x^{(m)},_\theta + u_\theta^{(m)},_x . \tag{20}$$

$$\boldsymbol{\sigma}_p^{(m)} = \mathbf{Q}_p^{(m)} \mathbf{B}_1 \mathbf{u}^{(m)} + \mathbf{Q}_p^{(m)} \mathbf{B}_2 u_r^{(m)} + \mathbf{Q}_r^{(m)} \sigma_r^{(m)} \tag{21}$$

where

$$\boldsymbol{\sigma}_p^{(m)} = \left\{ \begin{array}{ccc} \sigma_x^{(m)} & \sigma_\theta^{(m)} & \tau_{x\theta}^{(m)} \end{array} \right\}^T, \quad \mathbf{u}^{(m)} = \left\{ \begin{array}{cc} u_x^{(m)} & u_\theta^{(m)} \end{array} \right\}^T,$$

$$\mathbf{Q}_p^{(m)} = \begin{bmatrix} Q_{11}^{(m)} & Q_{12}^{(m)} & 0 \\ Q_{12}^{(m)} & Q_{22}^{(m)} & 0 \\ 0 & 0 & Q_{66}^{(m)} \end{bmatrix}, \quad \mathbf{B}_1 = \begin{bmatrix} \partial_x & 0 \\ 0 & r^{-1}\partial_\theta \\ r^{-1}\partial_\theta & \partial_x \end{bmatrix},$$

$$\mathbf{B}_2 = \begin{bmatrix} 0 \\ r^{-1} \\ 0 \end{bmatrix}, \quad \mathbf{Q}_r^{(m)} = \begin{bmatrix} Q_{13}^{(m)} \\ Q_{23}^{(m)} \\ 0 \end{bmatrix},$$

$$Q_{ij}^{(m)} = c_{ij}^{(m)} - \left(c_{i3}^{(m)} c_{j3}^{(m)}/c_{33}^{(m)}\right) \quad (i,j = 1,2 \text{ and } 6),$$

$$Q_{i3}^{(m)} = c_{i3}^{(m)}/c_{33}^{(m)} \quad (i = 1 \text{ and } 2).$$

3.2 Euler-Lagrange equations

Based on Hamilton's principle, we substitute Eqs. (15)-(21) into Eq. (11), impose the stationary principle of the RMVT-based Lagrangian energy functional (i.e., $\delta \int_{t_1}^{t_2} L_R\, dt = 0$), and then perform the integration by parts using Green's theorem, and finally obtain the Euler-Lagrange equations of 3D elasticity related to the free vibration problem of an axially loaded, multilayered FGM cylinder from the domain integral terms and the admissible boundary conditions from the boundary integral terms, which are written as follows:

The Euler-Lagrange equations are

$$\delta u_x^{(m)}:\ \tau_{xr}^{(m)},_{z_m} = -\sigma_x^{(m)},_x - \left(\tau_{x\theta}^{(m)},_\theta /r\right) - \left(\tau_{xr}^{(m)}/r\right) - \left(\bar{\sigma}_x^{(m)}\right)\left(u_x^{(m)},_{xx}\right) - \left(\bar{\sigma}_\theta^{(m)}\right)\left(u_x^{(m)},_{\theta\theta}/r^2\right) - (1/r)\left(\bar{\sigma}_r^{(m)} r u_x^{(m)},_r\right),_r + \rho^{(m)}\left(u_x^{(m)},_{tt}\right) \tag{22}$$

$$\delta u_\theta^{(m)}:\ \tau_{\theta r}^{(m)},_{z_m} = -\tau_{x\theta}^{(m)},_x - \left(\sigma_\theta^{(m)},_\theta /r\right) - 2\left(\tau_{\theta r}^{(m)}/r\right) - \left(\bar{\sigma}_x^{(m)}\right)\left(u_\theta^{(m)},_{xx}\right) - \left(\bar{\sigma}_\theta^{(m)}\right)\left(u_\theta^{(m)},_{\theta\theta} - u_\theta^{(m)} + 2u_r^{(m)},_\theta\right)/r^2 - (1/r)\left(\bar{\sigma}_r^{(m)} r u_\theta^{(m)},_r\right),_r + \rho^{(m)}\left(u_\theta^{(m)},_{tt}\right) \tag{23}$$

$$\delta u_r^{(m)}:\ \sigma_r^{(m)},_{z_m} = -\tau_{xr}^{(m)},_x - \left(\tau_{\theta r}^{(m)},_\theta /r\right) - \left(\sigma_r^{(m)}/r\right) + \left(\sigma_\theta^{(m)}/r\right) - \left(\bar{\sigma}_x^{(m)}\right)\left(u_r^{(m)},_{xx}\right) - \left(\bar{\sigma}_\theta^{(m)}\right)\left(-2u_\theta^{(m)},_\theta + u_r^{(m)},_{\theta\theta} - u_r^{(m)}\right)/r^2 - (1/r)\left(\bar{\sigma}_r^{(m)} r u_r^{(m)},_r\right),_r + \rho^{(m)}\left(u_r^{(m)},_{tt}\right) \tag{24}$$

$$\delta\tau_{xr}^{(m)}:\quad u_x^{(m)},_{z_m} = -u_r^{(m)},_x + \left(c_{55}^{(m)}\right)^{-1}\tau_{xr}^{(m)}, \tag{25}$$

$$\delta\tau_{\theta r}^{(m)}:\quad u_\theta^{(m)},_{z_m} = \left(u_\theta^{(m)}/r\right) - \left(u_r^{(m)},_\theta /r\right) + \left(c_{44}^{(m)}\right)^{-1}\tau_{\theta r}^{(m)}, \tag{26}$$

$$\delta\sigma_r^{(m)}:\quad u_r^{(m)},_{z_m} = -\left(c_{13}^{(m)}/c_{33}^{(m)}\right)u_x^{(m)},_x - \left(c_{23}^{(m)}/c_{33}^{(m)}\right)\left(u_\theta^{(m)},_\theta /r\right) - \left(c_{23}^{(m)}/c_{33}^{(m)}\right)\left(u_r^{(m)}/r\right) + \left(c_{33}^{(m)}\right)^{-1}\sigma_r^{(m)}, \tag{27}$$

where $m = 1,\ 2, \cdots, N_l$.

The lateral boundary conditions are

$$\begin{bmatrix}\tau_{xr}^{(N_l)} & \tau_{\theta r}^{(N_l)} & \sigma_r^{(N_l)}\end{bmatrix} = \begin{bmatrix}0 & 0 & 0\end{bmatrix} \quad \text{on} \quad z_{N_l} = h_{N_l}/2 \quad (\text{or } \zeta = H/2) \tag{28a}$$

$$\begin{bmatrix}\tau_{xr}^{(1)} & \tau_{\theta r}^{(1)} & \sigma_r^{(1)}\end{bmatrix} = \begin{bmatrix}0 & 0 & 0\end{bmatrix} \quad \text{on} \quad z_1 = -h_1/2 \quad (\text{or } \zeta = -H/2) \tag{28b}$$

The edge boundary conditions are

$$\sigma_x^{(m)} n_1 + \tau_{x\theta}^{(m)} n_2 = \bar{T}_x^{(m)} \quad \text{or} \quad u_x^{(m)} = \bar{u}_x^{(m)} \tag{29a}$$

$$\tau_{x\theta}^{(m)} n_1 + \sigma_{\theta}^{(m)} n_2 = \bar{T}_{\theta}^{(m)} \quad \text{or} \quad u_{\theta}^{(m)} = \bar{u}_{\theta}^{(m)} \tag{29b}$$

$$\tau_{xr}^{(m)} n_1 + \tau_{\theta r}^{(m)} n_2 = \bar{T}_{r}^{(m)} \quad \text{or} \quad u_{r}^{(m)} = \bar{u}_{r}^{(m)} \tag{29c}$$

where $m = 1,\ 2, \cdots, N_l$, and n_1 and n_2 stand for components of the unit normal vectors on the edges.

Discarding the inertia force terms in the above-mentioned Euler-Lagrange equations (Eqs. (22)-(27)) (i.e., $\rho^{(m)} u_k^{(m)}{}_{,tt} = 0$, in which $k = x, \theta$ and r) and redefining each variable as its incremental one perturbed from the state of neutral equilibrium, we may obtain the Euler-Lagrange equations governing the pure stability problems of the multilayered FGM cylinders. In contrast, while letting the applied compressive load vanish, we may obtain those governing the pure free vibration problems. The pure stability and free vibration problems of the cylinders can thus be included as special cases of the present RMVT-based formulation.

The set of Euler-Lagrange equations (Eqs. (22)-(27)) associated with a set of appropriate boundary conditions (Eqs. (29a, b, c)) is composed of a well-posed boundary value problem, which is the so-called strong formulation of this problem. A modified Pagano method will be developed for the 3D stability and free vibration analyses of a simply supported, multilayered FGM cylinder under axial compression later in this article on the basis of the strong formulation.

4 The modified Pagano method

4.1 Nondimensionalization

In order to scale all the field variables within a close order of magnitude and prevent unexpected numerical instabilities in the computation process, we define a set of dimensionless coordinates and variables, as follows:

$$x_1 = \frac{x}{\sqrt{Rh}}, \quad x_2 = \frac{\theta}{\sqrt{h/R}}, \quad x_3 = \frac{\zeta}{h},$$

$$u_1 = \frac{u_x}{\sqrt{Rh}}, \quad u_2 = \frac{u_\theta}{\sqrt{Rh}}, \quad u_3 = \frac{u_r}{R},$$

$$\sigma_1 = \frac{\sigma_x}{Q_0}, \quad \sigma_2 = \frac{\sigma_\theta}{Q_0}, \quad \tau_{xy} = \frac{\tau_{x\theta}}{Q_0},$$

$$\tau_{13} = \frac{\tau_{xr}}{Q_0\sqrt{h/R}}, \quad \tau_{23} = \frac{\tau_{\theta r}}{Q_0}, \quad \sigma_3 = \frac{\sigma_r R}{(Q_0 h)},$$

$$\bar{P}_x = \frac{P_x}{(2\pi RHQ_0)}, \quad \tau = \frac{(h\sqrt{Q_0})t}{(R^2\sqrt{P_0})} \tag{30a-n}$$

where h denotes the one-half total thickness of the cylinder (i.e., $h = H/2$); Q_0 and ρ_0 stand for the reference elastic coefficient and mass density, and are taken as the values of $Q_{11}^{(1)}$ and $\rho^{(1)}$ of the bottom layer of an N_l-layered cylinder in the illustrative examples of this article.

Introducing the set of dimensionless coordinates and variables given in Eq. ($30a-n$) in the formulation, and using the method of direct elimination, we obtain one set of state space equations in terms of the primary field variables, and these are given as follows:

$$\begin{aligned}
\frac{\partial}{\partial x_3}\begin{bmatrix} u_1^{(m)} \\ u_2^{(m)} \\ \sigma_3^{(m)} \\ \tau_{13}^{(m)} \\ \tau_{23}^{(m)} \\ u_3^{(m)} \end{bmatrix} &= \begin{bmatrix} 0 & 0 & 0 & k_{14}^{(m)} & 0 & k_{16}^{(m)} \\ 0 & k_{22}^{(m)} & 0 & 0 & k_{25}^{(m)} & k_{26}^{(m)} \\ k_{31}^{(m)} & k_{32}^{(m)} & k_{33}^{(m)} & k_{34}^{(m)} & k_{35}^{(m)} & k_{36}^{(m)} \\ k_{41}^{(m)} & k_{42}^{(m)} & k_{43}^{(m)} & k_{44}^{(m)} & 0 & k_{46}^{(m)} \\ k_{51}^{(m)} & k_{52}^{(m)} & k_{53}^{(m)} & 0 & k_{55}^{(m)} & k_{56}^{(m)} \\ k_{61}^{(m)} & k_{62}^{(m)} & k_{63}^{(m)} & 0 & 0 & k_{66}^{(m)} \end{bmatrix} \begin{bmatrix} u_1^{(m)} \\ u_2^{(m)} \\ \sigma_3^{(m)} \\ \tau_{13}^{(m)} \\ \tau_{23}^{(m)} \\ u_3^{(m)} \end{bmatrix} \\
&\quad - (\bar{p}_x) \begin{bmatrix} 0 & 0 & 0 & 0 & 0 & 0 \\ 0 & 0 & 0 & 0 & 0 & 0 \\ l_{31}^{(m)} & l_{32}^{(m)} & l_{33}^{(m)} & l_{34}^{(m)} & l_{35}^{(m)} & l_{36}^{(m)} \\ l_{41}^{(m)} & l_{42}^{(m)} & l_{43}^{(m)} & l_{44}^{(m)} & 0 & l_{46}^{(m)} \\ l_{51}^{(m)} & l_{52}^{(m)} & l_{53}^{(m)} & 0 & l_{55}^{(m)} & l_{56}^{(m)} \\ 0 & 0 & 0 & 0 & 0 & 0 \end{bmatrix} \begin{bmatrix} u_1^{(m)} \\ u_2^{(m)} \\ \sigma_3^{(m)} \\ \tau_{13}^{(m)} \\ \tau_{23}^{(m)} \\ u_3^{(m)} \end{bmatrix}, \qquad (31) \\
&\quad + \begin{bmatrix} 0 & 0 & 0 & 0 & 0 & 0 \\ 0 & 0 & 0 & 0 & 0 & 0 \\ 0 & 0 & 0 & 0 & 0 & \rho_1^{(m)}\partial_{\tau\tau} \\ \rho_2^{(m)}\partial_{\tau\tau} & 0 & 0 & 0 & 0 & 0 \\ 0 & \rho_2^{(m)}\partial_{\tau\tau} & 0 & 0 & 0 & 0 \\ 0 & 0 & 0 & 0 & 0 & 0 \end{bmatrix} \begin{bmatrix} u_1^{(m)} \\ u_2^{(m)} \\ \sigma_3^{(m)} \\ \tau_{13}^{(m)} \\ \tau_{23}^{(m)} \\ u_3^{(m)} \end{bmatrix}
\end{aligned}$$

where

$$k_{14}^{(m)} = \left(\tilde{c}_{55}^{(m)}\right)^{-1}(h/R), \quad k_{16}^{(m)} = -\partial_1, \quad k_{22}^{(m)} = (\gamma_2)^{-1}(h/R),$$

$$k_{25}^{(m)} = \left(\tilde{c}_{44}^{(m)}\right)^{-1}(h/R), \quad k_{26}^{(m)} = -(\gamma_2)^{-1}\partial_2, \quad k_{31}^{(m)} = c_3^{(m)}\tilde{Q}_{12}^{(m)}(\gamma_2)^{-1}\partial_1,$$

$$k_{32}^{(m)} = c_3^{(m)}\tilde{Q}_{22}^{(m)}(\gamma_2)^{-2}\partial_2, \quad k_{33}^{(m)} = c_3^{(m)}\left(Q_{23}^{(m)} - 1\right)(\gamma_2)^{-1}(h/R),$$

$$k_{34}^{(m)} = -c_3^{(m)}\partial_1, \quad k_{35}^{(m)} = -c_3^{(m)}(\gamma_2)^{-1}\partial_2, \quad k_{36}^{(m)} = c_3^{(m)}\tilde{Q}_{22}^{(m)}(\gamma_2)^{-2},$$

$$k_{41}^{(m)} = -c_4^{(m)}\left[\tilde{Q}_{11}^{(m)}\,\partial_{11} + \tilde{Q}_{66}^{(m)}\,(\gamma_2)^{-2}\,\partial_{22}\right],$$

$$k_{42}^{(m)} = -c_4^{(m)}\left[\left(\tilde{Q}_{12}^{(m)} + \tilde{Q}_{66}^{(m)}\right)(\gamma_2)^{-1}\right]\partial_{12}, \quad k_{43}^{(m)} = -c_4^{(m)}\left[Q_{13}^{(m)}\,(h/R)\right]\partial_1,$$

$$k_{44}^{(m)} = -c_4^{(m)}\left[(\gamma_2)^{-1}\,(h/R)\right], \quad k_{46}^{(m)} = -c_4^{(m)}\left[\tilde{Q}_{12}^{(m)}\,(\gamma_2)^{-1}\right]\partial_1,$$

$$k_{51}^{(m)} = -c_5^{(m)}\left[\left(\tilde{Q}_{12}^{(m)} + \tilde{Q}_{66}^{(m)}\right)(\gamma_2)^{-1}\right]\partial_{12},$$

$$k_{52}^{(m)} = -c_5^{(m)}\left[\tilde{Q}_{66}^{(m)}\,\partial_{11} + \tilde{Q}_{22}^{(m)}\,(\gamma_2)^{-2}\,\partial_{22}\right],$$

$$k_{53}^{(m)} = -c_5^{(m)}\left[Q_{23}^{(m)}\,(\gamma_2)^{-1}\,(h/R)\right]\partial_2, \quad k_{55}^{(m)} = -2\,c_5^{(m)}\,(\gamma_2)^{-1}\,(h/R),$$

$$k_{56}^{(m)} = -c_5^{(m)}\tilde{Q}_{22}^{(m)}\,(\gamma_2)^{-2}\,\partial_2, \quad k_{61}^{(m)} = -Q_{13}^{(m)}\,(h/R)\,\partial_1,$$

$$k_{62}^{(m)} = -Q_{23}^{(m)}\,(\gamma_2)^{-1}\,(h/R)\,\partial_2, \quad k_{63}^{(m)} = \left(\tilde{c}_{33}^{(m)}\right)^{-1}(h/R)^2,$$

$$k_{66}^{(m)} = -Q_{23}^{(m)}\,(\gamma_2)^{-1}\,(h/R),$$

$$l_{31}^{(m)} = c_3^{(m)}\left[Q_{13}^{(m)}\left(\hat{f}_r^{(m)},_3\right)(R/h) + Q_{13}^{(m)}\hat{f}_r^{(m)}\,(\gamma_2)^{-1} - Q_{13}^{(m)}Q_{23}^{(m)}\hat{f}_r^{(m)}\,(\gamma_2)^{-1}\right]\partial_1,$$

$$\begin{aligned} l_{32}^{(m)} =& c_3^{(m)}[2\hat{f}_\theta^{(m)}\,(\gamma_2)^{-2} + Q_{23}^{(m)}\left(\hat{f}_r^{(m)},_3\right)(\gamma_2)^{-1}\,(R/h) \\ &+ Q_{23}^{(m)}\hat{f}_r^{(m)}(\gamma_2)^{-2} - Q_{23}^{(m)}Q_{23}^{(m)}\hat{f}_r^{(m)}(\gamma_2)^{-2}]\partial_2 \end{aligned}$$

$$\begin{aligned} l_{33}^{(m)} =& c_3^{(m)}[-\left(\tilde{c}_{33}^{(m)}\right)^{-1}\left(\hat{f}_r^{(m)},_3\right) - \left(\tilde{c}_{33}^{(m)}\right)^{-1}\hat{f}_r^{(m)}(\gamma_2)^{-1}\,(h/R) \\ &+ \left(\tilde{c}_{33}^{(m)}\right)^{-1}Q_{23}^{(m)}\hat{f}_r^{(m)}(\gamma_2)^{-1}\,(h/R)] \end{aligned}$$

$$l_{34}^{(m)} = c_3^{(m)}\left[(\tilde{c}_{55})^{-1}\,Q_{13}^{(m)}\hat{f}_r^{(m)}\right]\partial_1, \quad l_{35}^{(m)} = c_3^{(m)}\left[(\tilde{c}_{44})^{-1}\,Q_{23}^{(m)}\hat{f}_r^{(m)}\,(\gamma_2)^{-1}\right]\partial_2,$$

$$\begin{aligned} l_{36}^{(m)} =& -c_3^{(m)}\left\{\left[\hat{f}_x^{(m)}\,(R/h) + Q_{13}^{(m)}\hat{f}_r^{(m)}\,(R/h)\right]\partial_{11}\right. \\ &+ \left[\hat{f}_\theta^{(m)}(\gamma_2)^{-2}\,(R/h) + Q_{23}^{(m)}\hat{f}_r^{(m)}(\gamma_2)^{-2}\,(R/h)\right]\partial_{22} \\ &\left.+ \left[-\hat{f}_\theta^{(m)}(\gamma_2)^{-2} - Q_{23}^{(m)}\left(\hat{f}_r^{(m)},_3\right)(\gamma_2)^{-1}(R/h) + Q_{23}^{(m)}Q_{23}^{(m)}\hat{f}_r^{(m)}(\gamma_2)^{-2}\right]\right\} \end{aligned}$$

$$l_{41}^{(m)} = -c_4^{(m)}\left\{\left(\hat{f}_x^{(m)} + Q_{13}^{(m)}\hat{f}_r^{(m)}\right)\partial_{11} + \left[\hat{f}_\theta^{(m)}\,(\gamma_2)^{-2}\right]\partial_{22}\right\},$$

$$l_{42}^{(m)} = -c_4^{(m)}\left[Q_{23}^{(m)}\hat{f}_r^{(m)}\,(\gamma_2)^{-1}\right]\partial_{12}, \quad l_{43}^{(m)} = c_4^{(m)}\left[\left(\tilde{c}_{33}^{(m)}\right)^{-1}\hat{f}_r^{(m)}\,(h/R)\right]\partial_1,$$

$$l_{44}^{(m)} = -c_4^{(m)}\left[\left(\tilde{c}_{55}^{(m)}\right)^{-1}\left(\hat{f}_r^{(m)},_3\right) + \left(\tilde{c}_{55}^{(m)}\right)^{-1}\hat{f}_r^{(m)}\,(\gamma_2)^{-1}\,(h/R)\right],$$

$$l_{46}^{(m)} = c_4^{(m)} \left[\left(\hat{f}_r^{(m)},_3 \right) (R/h) + \hat{f}_r^{(m)} (\gamma_2)^{-1} - Q_{23}^{(m)} \hat{f}_r^{(m)} (\gamma_2)^{-1} \right] \partial_1,$$

$$l_{51}^{(m)} = -c_5^{(m)} \left[Q_{13}^{(m)} \hat{f}_r^{(m)} (\gamma_2)^{-1} \right] \partial_{12},$$

$$\begin{aligned} l_{52}^{(m)} =& c_5^{(m)} \left\{ -\hat{f}_x^{(m)} \partial_{11} - \left[\hat{f}_\theta^{(m)} (\gamma_2)^{-2} + Q_{23}^{(m)} \hat{f}_r^{(m)} (\gamma_2)^{-2} \right] \partial_{22} \right. \\ & \left. + \left[\hat{f}_\theta^{(m)} (\gamma_2)^{-2} (h/R) - \left(\hat{f}_r^{(m)},_3 \right) (\gamma_2)^{-1} - \hat{f}_r^{(m)} (\gamma_2)^{-2} (h/R) \right] \right\}' \end{aligned}$$

$$l_{53}^{(m)} = c_5^{(m)} \left[\left(\tilde{c}_{33}^{(m)} \right)^{-1} \hat{f}_r^{(m)} (\gamma_2)^{-1} (h/R) \right] \partial_2,$$

$$l_{55}^{(m)} = -c_5^{(m)} \left[\left(\tilde{c}_{44}^{(m)} \right)^{-1} \left(\hat{f}_r^{(m)},_3 \right) + 2 \left(\tilde{c}_{44}^{(m)} \right)^{-1} \hat{f}_r^{(m)} (\gamma_2)^{-1} (h/R) \right],$$

$$l_{56}^{(m)} = c_5^{(m)} \left[-2\hat{f}_\theta^{(m)} (\gamma_2)^{-2} + \left(\hat{f}_r^{(m)},_3 \right) (R/h) + \hat{f}_r^{(m)} (\gamma_2)^{-2} - Q_{23}^{(m)} \hat{f}_r^{(m)} (\gamma_2)^{-2} \right] \partial_2,$$

$$c_3^{(m)} = 1 / \left[1 - \bar{p}_x \left(\tilde{c}_{33}^{(m)} \right)^{-1} \hat{f}_r^{(m)} \right], \quad c_4^{(m)} = 1 / \left[1 - \bar{p}_x \left(\tilde{c}_{55}^{(m)} \right)^{-1} \hat{f}_r^{(m)} \right],$$

$$c_5^{(m)} = 1 / \left[1 - \bar{p}_x \left(\tilde{c}_{44}^{(m)} \right)^{-1} \hat{f}_r^{(m)} \right],$$

$$\gamma_2 = 1 + (h x_3 / R), \quad \tilde{c}_{ij}^{(m)} = c_{ij}^{(m)} / Q_0 \quad (i, j = 1 - 6),$$

$$\tilde{Q}_{kl}^{(m)} = Q_{kl}^{(m)} / Q_0 \quad (k, l = 1, 2 \text{ and } 6),$$

$$Q_{13}^{(m)} = c_{13}^{(m)} / c_{33}^{(m)}, \quad Q_{23}^{(m)} = c_{23}^{(m)} / c_{33}^{(m)},$$

$$\rho_1^{(m)} = \left(\rho^{(m)} h^2 \right) / \left(\rho_0^{(m)} R^2 \right), \quad \rho_2^{(m)} = \left(\rho^{(m)} h^3 \right) / \left(\rho_0^{(m)} R^3 \right).$$

The dimensionless forms of the boundary conditions of the problem are specified as follows:

$$\tau_{13}^{(m)} = \tau_{23}^{(m)} = \sigma_3^{(m)} = 0 \quad \text{on} \quad x_3 = \pm 1. \tag{32}$$

At the edges, the following quantities are satisfied:

$$\sigma_1^{(m)} = u_2^{(m)} = u_3^{(m)} = 0, \quad \text{at} \quad x_1 = 0 \quad \text{and} \quad x_1 = L/\sqrt{Rh}. \tag{33}$$

4.2 The double Fourier series expansion method

The double Fourier series expansion method is applied to reduce the system of partial differential equations given in Eq. (31) to a system of ordinary differential ones, such that by means of satisfying the edge boundary conditions given in Eq. (33), the primary variables are expressed in the following forms:

$$\left(u_1^{(m)}, \quad \tau_{13}^{(m)}\right) = \sum_{\hat{m}=0}^{\infty}\sum_{\hat{n}=0}^{\infty}\left(u_{1\hat{m}\hat{n}}^{(m)}(x_3), \quad \tau_{13\hat{m}\hat{n}}^{(m)}(x_3)\right)\cos\tilde{m}x_1\cos\tilde{n}x_2\, e^{i\omega_\tau\tau}, \tag{34}$$

$$\left(u_2^{(m)}, \quad \tau_{23}^{(m)}\right) = \sum_{\hat{m}=0}^{\infty}\sum_{\hat{n}=0}^{\infty}\left(u_{2\hat{m}\hat{n}}^{(m)}(x_3), \quad \tau_{23\hat{m}\hat{n}}^{(m)}(x_3)\right)\sin\tilde{m}x_1\sin\tilde{n}x_2\, e^{i\omega_\tau\tau}, \tag{35}$$

$$\left(u_3^{(m)}, \ \sigma_3^{(m)}\right) = \sum_{\hat{m}=0}^{\infty}\sum_{\hat{n}=0}^{\infty}\left(u_{3\hat{m}\hat{n}}^{(m)}(x_3), \quad \sigma_{3\hat{m}\hat{n}}^{(m)}(x_3)\right)\sin\tilde{m}x_1\cos\tilde{n}x_2\, e^{i\omega_\tau\tau}, \tag{36}$$

where $\omega_\tau = \left(R^2\sqrt{\rho_0}\right)\omega/\left(h\sqrt{Q_0}\right)$, in which ω and ω_τ denote the natural frequency and its dimensionless form; $\tilde{m} = \hat{m}\pi\sqrt{Rh}/L$, $\tilde{n} = \hat{n}\sqrt{h/R}$, in which $\hat{m}$ and $\hat{n}$ are zeroes or positive integers.

For brevity, the symbols of summation are omitted in the following derivation. Using the set of dimensionless coordinates and field variables, which are given in Eq. (30), and substituting Eqs. (34)-(36) in Eq. (31), we have the resulting equations, as follows:

$$\frac{d\,\mathbf{F}^{(m)}(x_3)}{d\,x_3} = \bar{\mathbf{K}}^{(m)}\mathbf{F}^{(m)}(x_3), \tag{37}$$

where $\mathbf{F}^{(m)} = \left\{u_{1\hat{m}\hat{n}}^{(m)} \ u_{2\hat{m}\hat{n}}^{(m)} \ \sigma_{3\hat{m}\hat{n}}^{(m)} \ \tau_{13\hat{m}\hat{n}}^{(m)} \ \tau_{23\hat{m}\hat{n}}^{(m)} \ u_{3\hat{m}\hat{n}}^{(m)}\right\}^T$,

$$\bar{\mathbf{K}}^{(m)} = \begin{bmatrix} 0 & 0 & 0 & \bar{k}_{14}^{(m)} & 0 & \bar{k}_{16}^{(m)} \\ 0 & \bar{k}_{22}^{(m)} & 0 & 0 & \bar{k}_{25}^{(m)} & \bar{k}_{26}^{(m)} \\ \frac{\left(\bar{k}_{31}^{(m)}-\bar{p}_x\bar{l}_{31}^{(m)}\right)}{\left(1-\bar{p}_x\bar{l}_{30}^{(m)}\right)} & \frac{\left(\bar{k}_{32}^{(m)}-\bar{p}_x\bar{l}_{32}^{(m)}\right)}{\left(1-\bar{p}_x\bar{l}_{30}^{(m)}\right)} & \frac{\left(\bar{k}_{33}^{(m)}-\bar{p}_x\bar{l}_{33}^{(m)}\right)}{\left(1-\bar{p}_x\bar{l}_{30}^{(m)}\right)} & \frac{\left(\bar{k}_{34}^{(m)}-\bar{p}_x\bar{l}_{34}^{(m)}\right)}{\left(1-\bar{p}_x\bar{l}_{30}^{(m)}\right)} & \frac{\left(\bar{k}_{35}^{(m)}-\bar{p}_x\bar{l}_{35}^{(m)}\right)}{\left(1-\bar{p}_x\bar{l}_{30}^{(m)}\right)} & \frac{\left(\bar{k}_{36}^{(m)}-\bar{p}_x\bar{l}_{36}^{(m)}-\rho_1^{(m)}\omega_\tau^2\right)}{\left(1-\bar{p}_x\bar{l}_{30}^{(m)}\right)} \\ \frac{\left(\bar{k}_{41}^{(m)}-\bar{p}_x\bar{l}_{41}^{(m)}-\rho_2^{(m)}\omega_\tau^2\right)}{\left(1-\bar{p}_x\bar{l}_{40}^{(m)}\right)} & \frac{\left(\bar{k}_{42}^{(m)}-\bar{p}_x\bar{l}_{42}^{(m)}\right)}{\left(1-\bar{p}_x\bar{l}_{40}^{(m)}\right)} & \frac{\left(\bar{k}_{43}^{(m)}-\bar{p}_x\bar{l}_{43}^{(m)}\right)}{\left(1-\bar{p}_x\bar{l}_{40}^{(m)}\right)} & \frac{\left(\bar{k}_{44}^{(m)}-\bar{p}_x\bar{l}_{44}^{(m)}\right)}{\left(1-\bar{p}_x\bar{l}_{40}^{(m)}\right)} & 0 & \frac{\left(\bar{k}_{46}^{(m)}-\bar{p}_x\bar{l}_{46}^{(m)}\right)}{\left(1-\bar{p}_x\bar{l}_{40}^{(m)}\right)} \\ \frac{\left(\bar{k}_{51}^{(m)}-\bar{p}_x\bar{l}_{51}^{(m)}\right)}{\left(1-\bar{p}_x\bar{l}_{50}^{(m)}\right)} & \frac{\left(\bar{k}_{52}^{(m)}-\bar{p}_x\bar{l}_{52}^{(m)}-\rho_2^{(m)}\omega_\tau^2\right)}{\left(1-\bar{p}_x\bar{l}_{50}^{(m)}\right)} & \frac{\left(\bar{k}_{53}^{(m)}-\bar{p}_x\bar{l}_{53}^{(m)}\right)}{\left(1-\bar{p}_x\bar{l}_{50}^{(m)}\right)} & 0 & \frac{\left(\bar{k}_{55}^{(m)}-\bar{p}_x\bar{l}_{55}^{(m)}\right)}{\left(1-\bar{p}_x\bar{l}_{50}^{(m)}\right)} & \frac{\left(\bar{k}_{56}^{(m)}-\bar{p}_x\bar{l}_{56}^{(m)}\right)}{\left(1-\bar{p}_x\bar{l}_{50}^{(m)}\right)} \\ \bar{k}_{61}^{(m)} & \bar{k}_{62}^{(m)} & \bar{k}_{63}^{(m)} & 0 & 0 & \bar{k}_{66}^{(m)} \end{bmatrix}$$

in which $\bar{k}_{ij}^{(m)}$ and $\bar{l}_{ij}^{(m)}$ are given in Appendix A.

Equation (37) can then be used to investigate the free vibration problems of axially loaded and simply-supported, multilayered FGM/FRCM cylinders when the

applied axially compressive load is less than the corresponding critical one. As mentioned above, when the cylinders are unloaded (i.e., $\bar{p}_x = 0$), Eq. (37) will be reduced to the state space equations of the pure free vibration problems of the cylinders; while when the inertia force terms are discarded (i.e., $\omega_\tau = 0$) and each field variable is redefined as its incremental one perturbed from the state of neutral equilibrium, Eq. (37) will be reduced to those of the pure stability problems of the cylinders. The pure free vibration and stability problems can thus be regarded as special cases of this formulation. In addition, some effects on the lowest critical load parameters of the cylinders will be examined, such as the initial transverse normal stress effect, the deviations between using von K'arm'an's nonlinearity and the full kinematic one, and the ones between using the uniform initial stress assumption and the uniform initial strain one, and the corresponding system equations of each special case can be obtained using Eq. (37) with the reduced form of $\bar{\mathbf{K}}^{(m)}$, which are given as follows:

(A) Pure stability problems

(A-1) Without consideration of the effect of the initial transverse normal stress

When the inertia force terms are discarded and the effect of initial transverse normal stress is neglected in this formulation, which means $\omega_\tau = 0$ and $\hat{f}_r^{(m)} = 0$, the coefficient matrix $\bar{\mathbf{K}}^{(m)}$ given in Eq. (37) can be reduced as follows:

$$\bar{\mathbf{K}}^{(m)} = \begin{bmatrix} 0 & 0 & 0 & \bar{k}_{14}^{(m)} & 0 & \bar{k}_{16}^{(m)} \\ 0 & \bar{k}_{22}^{(m)} & 0 & 0 & \bar{k}_{25}^{(m)} & \bar{k}_{26}^{(m)} \\ \bar{k}_{31}^{(m)} & \left(\bar{k}_{32}^{(m)} - \bar{p}_x \tilde{l}_{32}^{(m)}\right) & \bar{k}_{33}^{(m)} & \bar{k}_{34}^{(m)} & \bar{k}_{35}^{(m)} & \left(\bar{k}_{36}^{(m)} - \bar{p}_x \tilde{l}_{36}^{(m)}\right) \\ \left(\bar{k}_{41}^{(m)} - \bar{p}_x \tilde{l}_{41}^{(m)}\right) & \bar{k}_{42}^{(m)} & \bar{k}_{43}^{(m)} & \bar{k}_{44}^{(m)} & 0 & \bar{k}_{46}^{(m)} \\ \bar{k}_{51}^{(m)} & \left(\bar{k}_{52}^{(m)} - \bar{p}_x \tilde{l}_{52}^{(m)}\right) & \bar{k}_{53}^{(m)} & 0 & \bar{k}_{55}^{(m)} & \left(\bar{k}_{56}^{(m)} - \bar{p}_x \tilde{l}_{56}^{(m)}\right) \\ \bar{k}_{61}^{(m)} & \bar{k}_{62}^{(m)} & \bar{k}_{63}^{(m)} & 0 & 0 & \bar{k}_{66}^{(m)} \end{bmatrix}, \tag{38}$$

in which $\tilde{l}_{ij}^{(m)}$ are given in Appendix A.

(A-2) The use of von K'arm'an's nonlinearity

When the inertia force terms are discarded and von K'arm'an's nonlinearity, rather than the full kinematics one, is considered, this means $\omega_\tau = 0$ is used and the terms $\hat{\varepsilon}_x^{(m)}$, $\hat{\varepsilon}_\theta^{(m)}$ and $\hat{\varepsilon}_r^{(m)}$ in Eqs. (14a-c) are reduced, as in the following forms:

$$\hat{\varepsilon}_x^{(m)} = (1/2)\left(u_r^{(m)},_x\right)^2,$$

$$\hat{\varepsilon}_{\theta}^{(m)} = \left(1/2\,r^2\right)\left[(u_r)^2 + \left(u_r^{(m)},_{\theta} - u_{\theta}\right)^2\right],$$

$$\hat{\varepsilon}_{r}^{(m)} = 0. \tag{39a-c}$$

Using Eq. (39) instead of Eq. (14), we may reduce the coefficient matrix $\bar{\mathbf{K}}^{(m)}$ given in Eq. (37) as follows:

$$\bar{\mathbf{K}}^{(m)} = \begin{bmatrix} 0 & 0 & 0 & \bar{k}_{14}^{(m)} & 0 & \bar{k}_{16}^{(m)} \\ 0 & \bar{k}_{22}^{(m)} & 0 & 0 & \bar{k}_{25}^{(m)} & \bar{k}_{26}^{(m)} \\ \bar{k}_{31}^{(m)} & \left(\bar{k}_{32}^{(m)} - \bar{p}_x\,\widehat{l}_{32}^{(m)}\right) & \bar{k}_{33}^{(m)} & \bar{k}_{34}^{(m)} & \bar{k}_{35}^{(m)} & \left(\bar{k}_{36}^{(m)} - \bar{p}_x\,\widehat{l}_{36}^{(m)}\right) \\ \bar{k}_{41}^{(m)} & \bar{k}_{42}^{(m)} & \bar{k}_{43}^{(m)} & \bar{k}_{44}^{(m)} & 0 & \bar{k}_{46}^{(m)} \\ \bar{k}_{51}^{(m)} & \left(\bar{k}_{52}^{(m)} - \bar{p}_x\,\widehat{l}_{52}^{(m)}\right) & \bar{k}_{53}^{(m)} & 0 & \bar{k}_{55}^{(m)} & \left(\bar{k}_{56}^{(m)} - \bar{p}_x\,\widehat{l}_{56}^{(m)}\right) \\ \bar{k}_{61}^{(m)} & \bar{k}_{62}^{(m)} & \bar{k}_{63}^{(m)} & 0 & 0 & \bar{k}_{66}^{(m)} \end{bmatrix}, \tag{40}$$

in which $\widehat{l}_{ij}^{(m)}$ are given in Appendix A.

(A-3) The use of a uniform initial stress assumption

When the inertia force terms are discarded and a uniform initial stress assumption, rather than a uniform strain assumption mentioned above, is taken to determine the initial state of stress, which means $\hat{f}_x^{(m)} = 1$ and $\hat{f}_{\theta}^{(m)} = \hat{f}_r^{(m)} = 0$, the coefficient matrix $\bar{\mathbf{K}}^{(m)}$ given in Eq. (37) can be reduced as follows:

$$\bar{\mathbf{K}}^{(m)} = \begin{bmatrix} 0 & 0 & 0 & \bar{k}_{14}^{(m)} & 0 & \bar{k}_{16}^{(m)} \\ 0 & \bar{k}_{22}^{(m)} & 0 & 0 & \bar{k}_{25}^{(m)} & \bar{k}_{26}^{(m)} \\ \bar{k}_{31}^{(m)} & \bar{k}_{32}^{(m)} & \bar{k}_{33}^{(m)} & \bar{k}_{34}^{(m)} & \bar{k}_{35}^{(m)} & \left(\bar{k}_{36}^{(m)} - \bar{p}_x\,\hat{l}_{36}^{(m)}\right) \\ \left(\bar{k}_{41}^{(m)} - \bar{p}_x\,\hat{l}_{41}^{(m)}\right) & \bar{k}_{42}^{(m)} & \bar{k}_{43}^{(m)} & \bar{k}_{44}^{(m)} & 0 & \bar{k}_{46}^{(m)} \\ \bar{k}_{51}^{(m)} & \left(\bar{k}_{52}^{(m)} - \bar{p}_x\,\hat{l}_{52}^{(m)}\right) & \bar{k}_{53}^{(m)} & 0 & \bar{k}_{55}^{(m)} & \bar{k}_{56}^{(m)} \\ \bar{k}_{61}^{(m)} & \bar{k}_{62}^{(m)} & \bar{k}_{63}^{(m)} & 0 & 0 & \bar{k}_{66}^{(m)} \end{bmatrix}, \tag{41}$$

in which $\hat{l}_{ij}^{(m)}$ are given in Appendix A.

(B) Pure free vibration problems

When the free vibration problems of a multilayered FGM cylinder without the applied compressive load is considered, which means $\bar{p}_x = 0$, the coefficient matrix

$\bar{\mathbf{K}}^{(m)}$ given in Eq. (37) can be reduced as follows:

$$\bar{\mathbf{K}}^{(m)} = \begin{bmatrix} 0 & 0 & 0 & \bar{k}_{14}^{(m)} & 0 & \bar{k}_{16}^{(m)} \\ 0 & \bar{k}_{22}^{(m)} & 0 & 0 & \bar{k}_{25}^{(m)} & \bar{k}_{26}^{(m)} \\ \bar{k}_{31}^{(m)} & \bar{k}_{32}^{(m)} & \bar{k}_{33}^{(m)} & \bar{k}_{34}^{(m)} & \bar{k}_{35}^{(m)} & \left(\bar{k}_{36}^{(m)} - \rho_1^{(m)}\,\omega_\tau^2\right) \\ \left(\bar{k}_{41}^{(m)} - \rho_2^{(m)}\,\omega_\tau^2\right) & \bar{k}_{42}^{(m)} & \bar{k}_{43}^{(m)} & \bar{k}_{44}^{(m)} & 0 & \bar{k}_{46}^{(m)} \\ \bar{k}_{51}^{(m)} & \left(\bar{k}_{52}^{(m)} - \rho_2^{(m)}\,\omega_\tau^2\right) & \bar{k}_{53}^{(m)} & 0 & \bar{k}_{55}^{(m)} & \bar{k}_{56}^{(m)} \\ \bar{k}_{61}^{(m)} & \bar{k}_{62}^{(m)} & \bar{k}_{63}^{(m)} & 0 & 0 & \bar{k}_{66}^{(m)} \end{bmatrix}. \tag{42}$$

Implementation of the above-mentioned RMVT-based formulation for each special case will be presented later in this work,

4.3 Theories of the homogeneous linear systems

Equation (37), which is a system of six simultaneously homogeneous ordinary differential equations in terms of six primary variables, represents the state space equations for the 3D stability and free vibration problems of a simply-supported, multilayered FGM circular hollow cylinder subjected to axial compression, and the general solution of this is

$$\mathbf{F}^{(m)} = \mathbf{\Omega}^{(m)}\,\mathbf{L}^{(m)}, \tag{43}$$

where $\mathbf{L}^{(m)}$ is a 6x1 matrix of arbitrary constants; $\mathbf{\Omega}^{(m)}$ is a fundamental matrix of Eq. (38), and is formed by six linearly independent solutions in the form of $\mathbf{\Omega}^{(m)} = \left[\mathbf{\Omega}_1^{(m)}, \mathbf{\Omega}_2^{(m)}, \cdots, \mathbf{\Omega}_6^{(m)}\right]$, in which $\mathbf{\Omega}_i^{(m)} = \mathbf{\Lambda}_i\, e^{\lambda_i x_3}$ (i=1,2, …, 6), and λ_i and $\mathbf{\Lambda}_i$ are the eigenvalues and their corresponding eigenvectors of the coefficient matrix $\bar{\mathbf{K}}^{(m)}$ in Eq. (37), respectively.

If the coefficient matrix $\bar{\mathbf{K}}^{(m)}$ has a complex eigenvalue λ_1 (i.e., $\lambda_1 = Re(\lambda_1) + iIm(\lambda_1)$), then its complex conjugate λ_2 (i.e., $\lambda_2 = Re(\lambda_1) - iIm(\lambda_1)$) is also an eigenvalue of $\bar{\mathbf{K}}^{(m)}$, due to the fact that all of the coefficients of $\bar{\mathbf{K}}^{(m)}$ are real. In addition, $\mathbf{\Lambda}_{1,2} = Re(\mathbf{\Lambda}_1) \pm iIm(\mathbf{\Lambda}_1)$ are the corresponding eigenvectors of the complex conjugate pair, (λ_1, λ_2). Using Euler's formula, we replace these complex-valued solutions with alternative two real-valued solutions to enhance computational efficiency, and these are given by

$$\mathbf{\Omega}_1^{(m)} = e^{Re(\lambda_1)x_3}\left[Re\,(\mathbf{\Lambda}_1)\ \cos\left(Im\,(\lambda_1)\,x_3\right) - Im\,(\mathbf{\Lambda}_1)\ \sin\left(Im\,(\lambda_1)\,x_3\right)\right], \tag{44a}$$

$$\mathbf{\Omega}_2^{(m)} = e^{Re(\lambda_1)x_3}\left[Re\,(\mathbf{\Lambda}_1)\ \sin\left(Im\,(\lambda_1)\,x_3\right) + Im\,(\mathbf{\Lambda}_1)\ \cos\left(Im\,(\lambda_1)\,x_3\right)\right]. \tag{44b}$$

On the basis of the previous set of linearly independent real-valued solutions, a transfer matrix method can be developed for the analysis of multilayered hollow cylinders, and it can be extended to the analysis of multilayered (or sandwiched) FGM ones using an SA method, where the FGM cylinder is artificially divided into a finite number (N_l) of individual layers with equal and small thicknesses for each layer, compared with the mid-surface radius, as well as with constant material properties, determined in an average thickness sense. The exact solutions of critical loads, natural frequencies and the associated field variables induced in the FGM cylinder can thus be gradually approached by increasing the number of individual layers.

4.4 The successive approximation method

This article undertakes the 3D stability and free vibration analyses of an axially loaded, FGM sandwich cylinder, which consists of an FGM core bounded with two homogeneous face sheets, one of the widely-utilized multilayered FGM cylinders, in which the thickness of each layer is h_i $(i = 1,\ 2\ \text{ and }\ 3$, and is counted from the bottom layer), $h_1 = h_3$ and $\sum_{i=1}^{3} h_i = H$; the material properties ($g_{ij}^{(m)}(\zeta)$ ($m = 1,\ 2$ and 3)) are assumed to be symmetric with respect to the mid-surface of the sandwich cylinder and continuous at the interfaces between adjacent layers, and obey a power-law distribution of the volume fractions of the constituents through the thickness coordinate, as follows:

$$g_{ij}^{(1)}(\zeta) = g_{ij}^{(f)} \qquad -h \le \zeta \le -(h_2/2), \tag{45a}$$

$$g_{ij}^{(2)}(\zeta) = g_{ij}^{(0)} + \left(g_{ij}^{(f)} - g_{ij}^{(0)}\right)\ \left[|\zeta|/(h_2/2)\right]^{\kappa_p} \qquad -(h_2/2) \le \zeta \le (h_2/2), \tag{45b}$$

$$g_{ij}^{(3)}(\zeta) = g_{ij}^{(f)} \qquad (h_2/2) \le \zeta \le h, \tag{45c}$$

where $g_{ij}^{(f)}$ and $g_{ij}^{(0)}$ denote the material properties of the face sheets and the reference material properties at the mid-surface of the cylinder, respectively; κ_p denotes the material-property gradient index, which represents the degree of the material gradient along the thickness coordinate, and it is apparent that when $\kappa_p = 0$, this FGM sandwich cylinder reduces to a single-layered homogeneous one with material properties, $g_{ij}^{(f)}$; while when $\kappa_p = \infty$, it reduces to a homogeneous sandwich cylinder, in which the material properties of the core and face-sheet layers are $g_{ij}^{(0)}$ and $g_{ij}^{(f)}$, respectively.

Because the material properties of the FGM core in an FGM sandwich cylinder vary along its thickness coordinate, resulting in a variant coefficient matrix in the

system equation (i.e., Eq. (37)), the conventional Pagano method can not be directly applied to this study of the FGM sandwich cylinder. An SA method is thus adopted to make the present approach feasible. In the SA method, the FGM sandwich cylinder is artificially divided into an N_l-layered cylinder with an equal and small thickness compared with the mid-surface radius, and with homogeneous material properties for each layer. For a typical m^{th}-layer in the upper half core layer of the cylinder, the material properties $g_{ij}^{(m)}$ are regarded as constants and are determined in an average thickness sense, as follows:

$$\begin{aligned}\bar{g}_{ij}^{(m)} &= \frac{1}{\Delta\zeta_m}\int_{\zeta_{m-1}}^{\zeta_m} g_{ij}(\zeta)\, d\zeta \\ &= g_{ij}^{(0)} + \frac{\left(g_{ij}^{(f)} - g_{ij}^{(0)}\right)}{(\kappa_p+1)\,(\Delta\zeta_m)\,(h_2/2)^{\kappa_p}}\left[(\zeta_m)^{(\kappa_p+1)} - (\zeta_{m-1})^{(\kappa_p+1)}\right],\end{aligned} \tag{46}$$

where $\Delta\zeta_m = \zeta_m - \zeta_{m-1}$.

By means of Eq. (46), the modified Pagano method can be extensively applied to this analysis of FGM sandwich cylinders. Increasing the number of artificial layers (N_l), we can approximate the exact solutions for the 3D stability and free vibration analyses of FGM sandwich cylinders to any desired accuracy.

4.5 The transfer matrix method

As we noted above, the modified Pagano method can be applied to the study of FGM sandwich cylinders using Eq. (46). The through-thickness distributions of material properties are modified as layerwise Heaviside functions, and the upper half of these are given by

$$g_{ij}(\zeta) = \sum_{m=1}^{N_l/2} \bar{g}_{ij}^{(m)}\left[S(\zeta-\zeta_{m-1}) - S(\zeta-\zeta_m)\right] \quad 0 \le \zeta \le (h_2/2), \tag{47a}$$

$$g_{ij}(\zeta) = g_{ij}^{(f)} \quad (h_2/2) \le \zeta \le h, \tag{47b}$$

where $S(\zeta)$ is the Heaviside step function, and the material properties of the lower half of the cylinder are symmetric to those of the upper half with respect to the mid-surface of the cylinder, which were given above and thus not repeated here.

A transfer matrix method for the analysis of the N_l-layered elastic cylinders is then used to obtain the critical loads and fundamental frequencies of the axially loaded and simply supported, multilayered FGM cylinders, and a detailed description of this is given in Appendix B.

5 Illustrative examples

5.1 Stability of orthotropic laminated cylinders

A benchmark problem with regard to the stability of a simply-supported, orthotropic laminated circular hollow cylinder subjected to axial compression is used here to validate the accuracy and convergence of the modified Pagano method in Table 1, in which the four- and eight-layered symmetric orthotropic cylinders (i.e., $[0^0/90^0]_s$ and $[0^0/90^0/0^0/90^0]_s$) are considered. The material properties of each layer are taken to be E_L/E_T=5, 10, 20, 30 and 40, $G_{LT}/E_T = 0.6$, $G_{TT}/E_T = 0.5$ and $\upsilon_{LT} = \upsilon_{TT} = 0.25$, in which the subscripts L and T denote the directions parallel and perpendicular to the fiber direction, and the geometric parameters of the cylinders are L/R=5 and R/H=5. The dimensionless critical load parameter is defined as $(\bar{P}_x)_{cr} = (P_x)_{cr}/(2\pi R E_T H)$. It can be seen in Table 1 that the present solutions of critical load parameters for $[0^0/90^0]_s$ and $[0^0/90^0/0^0/90^0]_s$ laminated cylinders converge when the number of divided layers (N_l) is taken to be eight, and the convergent solutions are in excellent agreement with those obtained using the layerwise fourth-order mixed model (LM4) developed by D'Ottavio and Carrera (2010). In Table 1, the 40-layer solutions with the superscripts a, b and c represent that these were obtained without consideration of the initial transverse normal stress, using von K'arm'an's nonlinearity instead of the full kinematic one, and using a uniform initial stress assumption instead of a uniform initial strain one, respectively. It is shown that even for a thick cylinder (R/H=5), the effect of the initial transverse normal stress ($\bar{\sigma}_r^{(m)}$) on the critical load parameters of the axially loaded cylinders is relatively minor, and the relative error between the 40-layer solutions with and without consideration of the effect is less than 0.07%. The 40-layer solutions based on a uniform initial strain assumption is slightly less than those based on a uniform initial stress one, and the deviation between them is less than 0.25% for a thick cylinder; the 40-layer solutions obtained using full kinematic nonlinearity are about 25% less than those obtained using von K'arm'an's one, and this is thus not recommended for the stability analysis of thick cylinders, and this observation about the effect of von K'arm'an's nonlinearity was also found by D'Ottavio and Carrera (2010) using the FSDT. The 40-layer solutions of the critical load parameters were also compared with those obtained by D'Ottavio and Carrera (2010) using a variety of refined and advanced 2D shell theories, such as the FSDT, the global second- and fourth-order displacement models (ED2 and ED4), the global fourth-order mixed model with a zig-zag function (EMZ4), the layerwise second-order displacement model (LD2), and LM4. It can be seen that the accuracy among these theories is LM4 > (LD2, EMZ4) > (ED4) > (ED2) > FSDT, in which ">" represents more accurate. Moreover, the critical load parameter increases when the

orthotropic ratio (E_L/E_T) becomes larger and E_T remains the same, which means the cylinder becomes stiffer.

Table 2 shows the solutions of the critical load parameters of $[0^0/90^0]_s$ and $[0^0/90^0/0^0/90^0]_s$ laminated cylinders, in which the radius-to-thickness ratio (R/H) is taken to be 5, 10, 20, 50 and 100; $E_L/E_T = 30$and L/R=5; the number of divided layers (N_l) is N_l=4, 8, 16, 32 and 40 for the $[0^0/90^0]_s$ cylinders, and N_l=8, 16, 32 and 40 for the $[0^0/90^0/0^0/90^0]_s$ ones. Again, it can be seen in Table 2 that the effect of initial transverse normal stress on the critical load parameters of the cylinders is relatively minor for both the thick and thin cylinders, that the present modified Pagano solutions using a uniform initial strain and stress assumptions closely agree to each other, and that the assumption of von K'arm'an's nonlinearity is appropriate for very thin cylinders (R/h=100), in which the relative errors are about 2%, as compared with the solutions obtained using the full kinematic nonlinearity, while this is unsuitable for the thin and thick cylinders (i.e., R/h=20 and $R/h > 10$), in which the relative errors are up to about 10% and greater than 25%, respectively. In addition, it is also shown that the lowest critical load parameters increase when the cylinders become thicker, and the buckling mode corresponding to the lowest critical load varies with changing the radius-to-thickness ratio.

Figures 2(a) and (b) show the variations of the present convergent solutions of the critical load parameter of axially loaded, laminated $[0^0/90^0]_s$ and $[0^0/90^0/0^0/90^0]_s$ cylinders, respectively, with the length-to-radius ratio for different values of the half-wave number $\hat{m}$, which is set at $\hat{m}$=1-5, in which $E_L/E_T = 30$, R/H=20, L/R=2-20, and the other material properties and critical load parameter are the same as those in Tables 1 and 2. Referring to these figures, the magnitude of the lowest critical load parameter and its corresponding number of half-waves ($\hat{m}$) for a wide range of length-to-radius (L/R) ratios are shown using a solid dark line, and can readily be found for any value of the L/R ratio. It is also shown that the critical buckling mode in the axial direction varies significantly with the length-to-radius ratio.

5.2 Stability of FGM sandwich cylinders

The stability of simply-supported, sandwich FGM cylinders consisting of a soft FGM core layer bounded with two stiff homogeneous face sheets (i.e., [homogeneous layer/FGM layer/homogeneous layer] cylinders), subjected to an axial compressive load, is examined in this section. The dimensionless critical load parameters are defined as $(\bar{P}_x)_{cr} = (P_x)_{cr} R^2/\left(2\pi R E_f H^3\right)$, in which E_f denotes the Young's modulus of the face sheets. The thickness ratio of each layer of the sandwich cylinder is $h_1 : h_2 : h_3$, in which $h_1 = h_3$ and $\sum_{m=1}^{3} h_m = H$, while the effective

Table 1: The effect of the orthotropic ratio on the critical load parameters of orthotropic laminated cylinders under axial compression (L/R=5, R/H =5, and $(\bar{P}_x)_{cr} = (P_x)_{cr} / (2\pi R E_T H)$).

Laminates	$(\hat{m},\hat{n})$	Theories	E_L/E_T				
			5	10	20	30	40
$[0^0/90^0]_s$	(2, 2)	LM4	0.1377	0.1757	0.2275	0.2667	0.2992
		LD2	0.1377	0.1759	0.2282	0.2681	0.3014
		EMZ4	0.1377	0.1759	0.2281	0.2679	0.3011
		ED4	0.1377	0.1758	0.2282	0.2682	0.3016
		ED2	0.1385	0.1778	0.2330	0.2767	0.3144
		FSDT (nonlinear)	0.1385	0.1770	0.2305	0.2721	0.3075
		FSDT	0.1735	0.2211	0.2880	0.3401	0.3844
		Present ($N_l = 4$)	0.1375	0.1754	0.2270	0.2661	0.2985
		Present ($N_l = 8$)	0.1375	0.1754	0.2270	0.2661	0.2986
		Present ($N_l = 16$)	0.1375	0.1754	0.2270	0.2662	0.2986
		Present ($N_l = 32$)	0.1375	0.1754	0.2270	0.2662	0.2986
		Present ($N_l = 40$)	0.1375	0.1754	0.2270	0.2662	0.2986
		[a]Present ($N_l = 40$)	0.1374	0.1754	0.2272	0.2664	0.2988
		[b]Present ($N_l = 40$)	0.1729	0.2200	0.2848	0.3340	0.3747
		[c]Present ($N_l = 40$)	0.1377	0.1757	0.2275	0.2667	0.2992
$[0^0/90^0/0^0/90^0]_s$	(3, 2)	LM4	0.1581	0.2005	0.2601	0.3042	0.3393
		LD2	0.1581	0.2005	0.2601	0.3043	0.3393
		EMZ4	0.1581	0.2006	0.2605	0.3049	0.3403
		ED4	0.1581	0.2007	0.2607	0.3054	0.3410
		ED2	0.1592	0.2033	0.2671	0.3161	0.3561
		FSDT (nonlinear)	0.1586	0.2012	0.2614	0.3064	0.3425
		FSDT	0.1939	0.2480	0.3245	0.3813	0.4268
		Present ($N_l = 8$)	0.1577	0.2000	0.2596	0.3037	0.3388
		Present ($N_l = 16$)	0.1577	0.2000	0.2596	0.3037	0.3388
		Present ($N_l = 32$)	0.1577	0.2000	0.2596	0.3037	0.3388
		Present ($N_l = 40$)	0.1577	0.2000	0.2596	0.3037	0.3388
		[a]Present ($N_l = 40$)	0.1578	0.2002	0.2598	0.3039	0.3390
		[b]Present ($N_l = 40$)	0.1934	0.2474	0.3231	0.3788	0.4229
		[c]Present ($N_l = 40$)	0.1581	0.2005	0.2601	0.3042	0.3393
[a]The present solutions obtained without considerations of the initial transverse normal stress.							
[b]The present solutions obtained using the von Karman's nonlinearity.							
[c]The present solutions obtained using a uniform stress assumption for the state of initial stresses.							

Table 2: The effect of the radius-to-thickness ratio on the critical load parameters of orthotropic laminated cylinders under axial compression ($E_L/E_T = 30$, L/R=5, and $(\bar{P}_x)_{cr} = (P_x)_{cr} / (2\pi R E_T H)$).

Laminates	Theories	*R/H*				
		5	10	20	50	100
$[0^0/90^0]_s$	$(\hat{m},\ \hat{n})$	(2, 2)	(2, 2)	(3, 3)	(5, 5)	(7, 7)
	Present ($N_l = 4$)	0.2661	0.1563	0.09016	0.03967	0.02053
	Present ($N_l = 8$)	0.2661	0.1563	0.09015	0.03967	0.02052
	Present ($N_l = 16$)	0.2662	0.1563	0.09015	0.03967	0.02052
	Present ($N_l = 32$)	0.2662	0.1563	0.09015	0.03967	0.02052
	Present ($N_l = 40$)	0.2662	0.1563	0.09015	0.03967	0.02052
	[a]Present ($N_l = 40$)	0.2664	0.1563	0.09017	0.03967	0.02053
	[b]Present ($N_l = 40$)	0.3340	0.1951	0.10020	0.04129	0.02095
	[c]Present ($N_l = 40$)	0.2667	0.1564	0.09023	0.03969	0.02053
$[0^0/90^0/0^0/90^0]_s$	$(\hat{m},\ \hat{n})$	(1, 1)	(2, 2)	(4, 3)	(6, 5)	(9, 7)
	Present ($N_l = 8$)	0.2886	0.1692	0.1013	0.04551	0.02348
	Present ($N_l = 16$)	0.2887	0.1692	0.1013	0.04551	0.02348
	Present ($N_l = 32$)	0.2887	0.1692	0.1013	0.04551	0.02348
	Present ($N_l = 40$)	0.2887	0.1692	0.1013	0.04551	0.02348
	[a]Present ($N_l = 40$)	0.2879	0.1693	0.1013	0.04551	0.02348
	[b]Present ($N_l = 40$)	0.3788	0.2112	0.1124	0.04733	0.02396
	[c]Present ($N_l = 40$)	0.2880	0.1693	0.1014	0.04552	0.02348
[a]The present solutions obtained without considerations of the initial transverse normal stress.						
[b]The present solutions obtained using the von Karman's nonlinearity.						
[c]The present solutions obtained using a uniform stress assumption for the state of initial stresses.						

engineering constants of each layer are written as follows:

$$E^{(m)}(\zeta) = E_0 + (E_f - E_0)\,\Gamma^{(m)}(\zeta) \quad (m = 1, 2 \text{ and } 3), \tag{48a}$$

$$\upsilon^{(m)} = \text{constant} \quad (m = 1, 2 \text{ and } 3), \tag{48b}$$

where E_0 denotes the Young's modulus of the material at the mid-surface of the core, for which E_0=70 GPa (aluminum) and E_f=380 GPa (alumina) are used in this example; $\upsilon^{(m)}$ (m=1-3) are taken to be 0.3; $\Gamma^{(m)}$ (m=1-3) are the volume fractions of the constituents of the cylinder, and are given by

$$\Gamma^{(1)} = 1 \quad \text{when} \quad (-H/2) \le \zeta \le (-h_2/2), \tag{49a}$$

$$\Gamma^{(2)}(\zeta) = [\,|\zeta|\,/\,(h_2/2)\,]^{\kappa_p} \quad \text{when} \quad (-h_2/2) < \zeta < (h_2/2), \tag{49b}$$

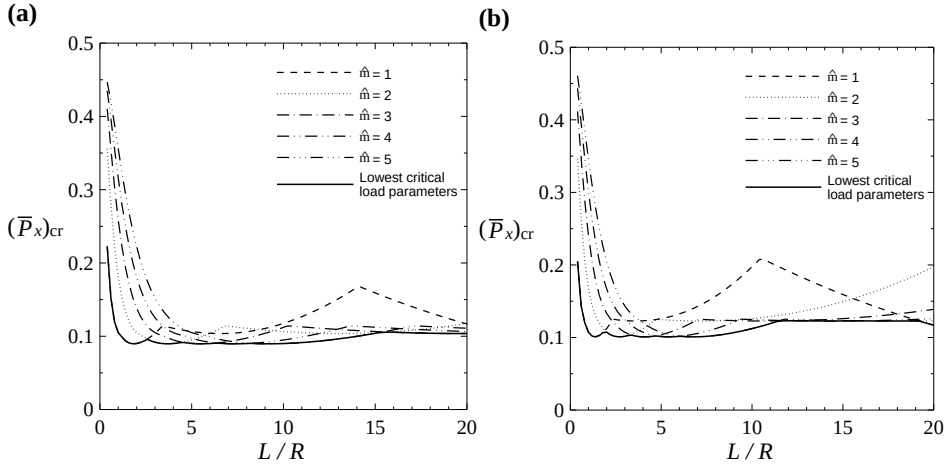

Figure 2: Variations of the critical load parameters of axially loaded, laminated orthotropic cylinders with the length-to-radius ratio, (a) $\left[0^0/90^0\right]_S$laminated cylinders, (b) $\left[0^0/90^0/0^0/90^0\right]_S$ laminated cylinders.

$$\Gamma^{(3)}=1 \quad \text{when} \quad (h_2/2)\le\zeta\le(H/2)\,, \tag{49c}$$

where κ_p denotes the material-property gradient index.

It is apparent that when κ_p=0, $\Gamma^{(2)}=1$, this FGM sandwich cylinder reduces to a single-layered homogeneous cylinder with material properties E_f=380 GPa and υ_f=0.3; while when $\kappa_p=\infty$, $\Gamma^{(2)}=0$, this FGM sandwich cylinder reduces to a homogeneous sandwich cylinder with material properties $E^{(1)}=E^{(3)}$=380 GPa, $E^{(2)}$=70 GPa, and $\upsilon^{(m)}$=0.3 (m=1-3).

Table 3 shows the solutions of the lowest critical load parameters of axially loaded, FGM sandwich cylinders with different values of the thickness ratio for each layer and the material-property gradient index, in which N_l=10, 20, 40 and 80; L/R=5 and R/H=10; $h_1:h_2:h_3=0.1H:0.8H:0.1H$, $0.2H:0.6H:0.2H$, $H/3:H/3:H/3$ and $0.4H:0.2H:0.4H$; κ_p= 0, 1, 5, 10, 100 and ∞. It can be seen in Table 3 that the solutions converge rapidly, the relative error between the 20-layer solution and 80-layer one is less than 0.6%, and it is less than 0.2% between the 40-layer solution and 80-layer one. The lowest critical load parameter decreases when the material-property gradient index and core/face sheet thickness ratio become larger, which means that the cylinder becomes softer. The critical buckling mode of these cylinders always occur at $(\hat{m},\,\hat{n})=(1,\,2)$, which means this will not be affected by changing the values of the material-property gradient index and the thickness ratio for each layer for the specific length-to-radius and radius-to-thickness ratios.

Table 3: The effects of the thickness ratio for each layer and the material-property gradient index on the critical load parameters of FGM sandwich cylinders under axial compression (L/R=5, R/H=10, and $(\bar{P}_x)_{cr} = (P_x)_{cr} R^2 / \left(2\pi R E_f H^3\right)$).

$h_1 : h_2 : h_3$	$(\hat{m}, \hat{n})$	Theories	κ_p					
			0	1	5	10	100	∞
$0.1H$:$0.8H$:$0.1H$	(1, 2)	Present ($N_l = 10$)	3.5856	2.8214	2.148	1.9534	1.7173	1.6859
		Present ($N_l = 20$)	3.5855	2.8296	2.1571	1.9607	1.7173	1.6859
		Present ($N_l = 40$)	3.5854	2.8316	2.1596	1.9634	1.7177	1.6859
		Present ($N_l = 80$)	3.5854	2.8321	2.1603	1.9642	1.7185	1.6859
$0.2H$:$0.6H$:$0.2H$	(1, 2)	Present ($N_l = 10$)	3.5856	3.0760	2.6696	2.5686	2.4206	2.3978
		Present ($N_l = 20$)	3.5855	3.0814	2.6658	2.5554	2.4206	2.3978
		Present ($N_l = 40$)	3.5854	3.0826	2.6652	2.5523	2.4201	2.3978
		Present ($N_l = 80$)	3.5854	3.0830	2.6650	2.5516	2.4183	2.3978
$H/3$:$H/3$:$H/3$	(1, 2)	Present ($N_l = 9$)	3.5857	3.3548	3.1842	3.1332	3.0452	3.0344
		Present ($N_l = 18$)	3.5855	3.3365	3.1543	3.1145	3.0455	3.0343
		Present ($N_l = 39$)	3.5854	3.3375	3.1462	3.1002	3.0454	3.0342
		Present ($N_l = 78$)	3.5854	3.3368	3.1445	3.0968	3.0450	3.0342
$0.4H$:$0.2H$:$0.4H$	(1, 2)	Present ($N_l = 10$)	3.5856	3.4421	3.3727	3.3301	3.2775	3.2723
		Present ($N_l = 20$)	3.5855	3.4421	3.3478	3.3247	3.2784	3.2722
		Present ($N_l = 40$)	3.5854	3.4417	3.3361	3.3129	3.2785	3.2721
		Present ($N_l = 80$)	3.5854	3.4415	3.3331	3.3074	3.2784	3.2721

Figure 3 shows the variations of the 40-layer solutions of the critical load parameter $((\bar{P}_x)_{cr})$ of axially loaded, FGM sandwich cylinders with the length-to-radius ratio, for $\hat{m} = 1 - 5$, in which R/H=20, $\kappa_p = 1,\ 5$ and 100, and $h_1 : h_2 : h_3 = 0.2H : 0.6H : 0.2H$. Again, referring to this figure, the magnitude of the lowest critical load parameter and its corresponding number of half-waves ($\hat{m}$) for a wide range of length-to-radius ratios are shown using a solid dark line and can be readily found. It can be seen that the lowest critical load decreases as the material-property gradient index (κ_p) becomes larger, while the corresponding buckling modes are not affected by changing the values of κ_p.

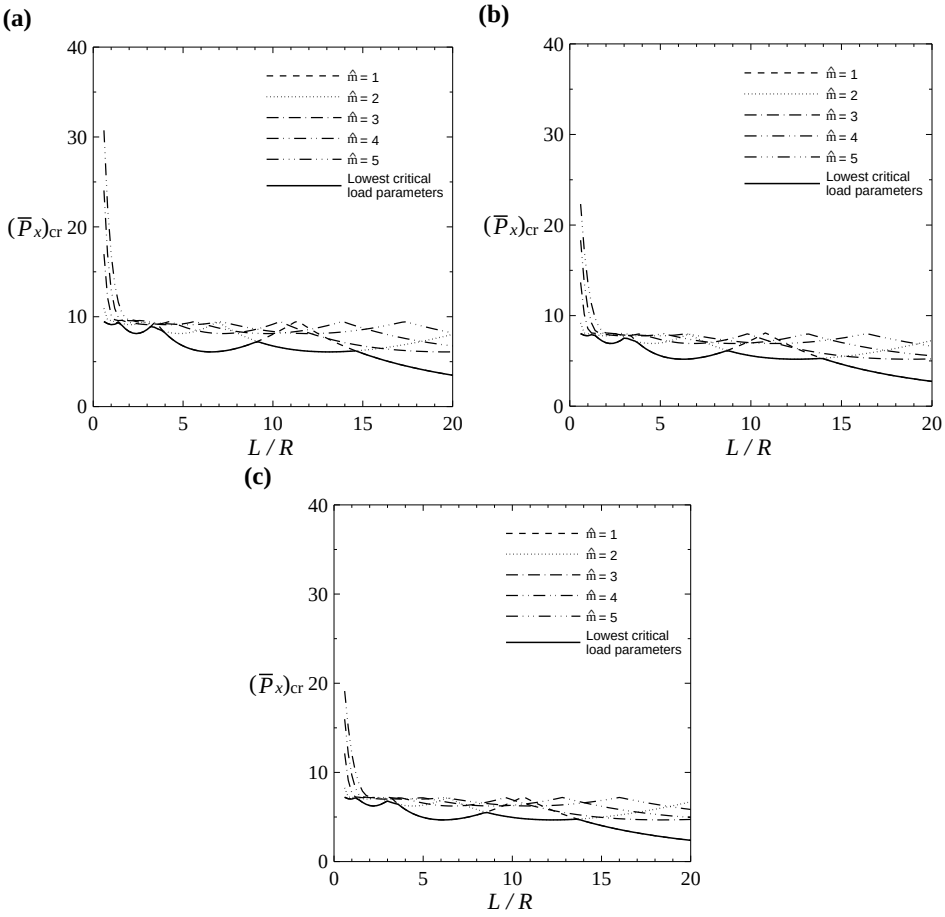

Figure 3: Variations of the critical load parameters of axially loaded, FGM sandwich cylinders with the length-to-radius ratio, (a) $\kappa_p = 1$, (b) $\kappa_p = 5$, (c) $\kappa_p = 100$.

5.3 Free vibration of axially loaded, laminated orthotropic cylinders

A benchmark problem with regard to the free vibration of a simply-supported, laminated orthotropic circular hollow cylinder without any axial compression, is used here to validate the accuracy and convergence of the modified Pagano method in Table 4, in which two-layered antisymmetric and four-layered symmetric orthotropic cylinders (i.e., $[0^0/90^0]$ and $[90^0/0^0/0^0/90^0]$) are considered. The material properties of each layer are taken to be E_L/E_T=3, 10 and 40, $G_{LT}/E_T = 0.6$, $G_{TT}/E_T = 0.5$ and $\upsilon_{LT} = \upsilon_{TT} = 0.25$, the geometric parameters of the cylinders are L/R=1 and R/H=5, and the dimensionless frequency parameter is defined as

$\bar{\omega} = \omega\,(10)\,\sqrt{\rho\,H^2/E_T}$.

Table 4: Convergence study of the present modified Pagano solutions of the natural frequency parameters of simply supported, laminated orthotropic cylinders with different values of E_L/E_T ($\hat{m} = 1,\ \hat{n} = 2$, *L*/*R*=1, *R*/*H*=5, $P_x = 0$ and $\bar{\omega} = \omega\,(10)\,\sqrt{\rho\,H^2/E_T}$).

Theories	$[0^0/90^0]$		
	$E_L/E_T = 3$	$E_L/E_T = 10$	$E_L/E_T = 40$
LM1	2.3217	2.5538	2.9328
LD2	2.315	2.5514	2.9594
LD1	2.3292	2.5626	2.9666
ED2	2.3219	2.5589	2.9822
ED1	2.345	2.5826	3.0367
3D solutions	2.3141	2.5464	2.9262
EFG	2.3141	2.5464	2.9263
Present ($N_l = 4$)	2.3143	2.5464	2.9262
Present ($N_l = 8$)	2.3141	2.5464	2.9263
Present ($N_l = 16$)	2.3141	2.5464	2.9263
Present ($N_l = 32$)	2.3141	2.5464	2.9263
Present ($N_l = 40$)	2.3141	2.5464	2.9263
Theories	$[90^0/0^0/0^0/90^0]$		
	$E_L/E_T = 3$	$E_L/E_T = 10$	$E_L/E_T = 40$
LM1	2.3153	2.6472	3.1358
LD2	2.3181	2.6589	3.1979
LD1	2.3522	2.6665	3.2087
ED2	2.3266	2.6842	3.3205
ED1	2.3577	2.7066	3.3322
3D solutions	2.3173	2.6542	3.1675
EFG	2.3172	2.6542	3.1676
Present ($N_l = 4$)	2.3175	2.654	3.1669
Present ($N_l = 8$)	2.3174	2.6542	3.1674
Present ($N_l = 16$)	2.3173	2.6542	3.1676
Present ($N_l = 32$)	2.3173	2.6542	3.1676
Present ($N_l = 40$)	2.3173	2.6542	3.1676

Table 4 shows the convergence studies for the solutions of least frequency parameters of $[0^0/90^0]$ and $[90^0/0^0/0^0/90^0]$ laminated cylinders, in which the number of layers (N_l) is N_l=4, 8, 16, 32 and 40, and $(\hat{m},\ \hat{n}) = (1,\ 2)$. It can be seen in Table 4 that the solutions are accurate and converge rapidly, and when N_l=8,

these are in excellent agreement with the exact 3D solutions obtained by Noor and Rarig (1974) and approximate 3D solutions obtained using the RMVT-based element free Galerkin (EFG) method by Wu and Yang (2011). The present solutions are also compared with the available results obtained from the global first-order displacement model (ED1) and the ED2 model, the layerwise first-order displacement model (LD1) and the LD2 model, and the layerwise first- and second-order mixed models (LM1 and LM2), which were given by Carrera (2003). It is seen in Table 4 that the performance among these theories is LM>LD>ED on the basis of the same orders of field variables. In addition, the fundamental frequency parameters increase when the ratio of E_L/E_T of the lamina becomes larger, which implies the cylinders with a high ratio of E_L/E_T possess high overall stiffness, thus increasing their corresponding frequency parameters, and the frequency parameters of the four-layered symmetric cylinders ($[90^0/0^0/0^0/90^0]$) are higher than the two-layered anti-symmetric ones ($[0^0/90^0]$), which implies that the coupling extension-bending effect of anti-symmetric cylinders decreases their overall stiffness, thus decreasing their corresponding frequency parameters.

Table 5 shows the present solutions of the lowest frequency parameters of axially loaded and simply supported, laminated four- and eight-layered symmetric orthotropic cylinders (i.e., $[0^0/90^0]_s$ and $[0^0/90^0/0^0/90^0]_s$) with different values of the compressive load, in which the frequency and parameter is defined as those in Table 4 and $(\bar{P}_x)_{cr} = (P_x)_{cr} R^2/(2\pi R H^3 E_T)$; N_l=4, 8, 16, 32 and 40; R/H=5, 10, 20 and 100, and L/R=5; E_L/E_T=40, and other material properties are the same as those in Table 4; P_x= 0, 0.2 $(P_x)_{cr}$, 0.5 $(P_x)_{cr}$ and 0.8 $(P_x)_{cr}$. It can be seen that the convergent solutions are obtained at N_l=8, and the lowest frequency parameter decreases when the magnitude of the compressive load becomes larger and when the cylinder becomes thinner. The vibration mode associated with the lowest frequency parameter remains the same with changing the magnitude of the compressive load, and in most of the cases considered, the half-wave numbers, ($\hat{m}$, $\hat{n}$), associated with the lowest frequency and critical load parameters are usually not identical to each other.

5.4 Free vibration of axially loaded, FGM sandwich cylinders

The free vibration of axially loaded and simply supported, FGM sandwich circular hollow cylinders, which consist of two homogeneous face-sheets and an FGM core, is studied in this section. The dimensionless frequency parameter is defined as $\bar{\omega} = \omega\,(10)\sqrt{\rho_f H^2/E_f}$, the Young's modulus ($E$) and Poisson's ratio ($\upsilon$) of face sheets and core are given in Eq. (48), and the mass densities of these are given as follows:

$$\rho^{(m)}(\zeta) = \rho_0 + (\rho_f - \rho_0)\ \Gamma^{(m)}(\zeta), \tag{50}$$

Table 5: The present modified Pagano solutions of the lowest frequency and critical load parameters of axially loaded and simply supported, laminated orthotropic cylinders with different values of the compressive load (L/R=5, $E_L/E_T = 40$, $\bar{\omega} = \omega\ (10)\ \sqrt{\rho H^2/E_T}$ and $(\bar{P}_x)_{cr} = (P_x)_{cr} R^2/\left(2\pi\, R E_T H^3\right)$).

Laminates	R/H	Present	$\bar{\omega}$ $(P_x = 0)$	$\bar{\omega}$ $(P_x = 0.2\ (P_x)_{cr})$	$\bar{\omega}$ $(P_x = 0.5\ (P_x)_{cr})$	$\bar{\omega}$ $(P_x = 0.8\ (P_x)_{cr})$	$(\bar{P}_x)_{cr}$ (Pure stability)
$\left[0^0/90^0\right]_s$	5	$(\hat{m},\hat{n})$	(1, 1)	(1, 1)	(1, 1)	(1, 1)	(2, 2)
		$N_l = 4$	0.6912	0.6194	0.4922	0.3177	7.4630
		$N_l = 8$	0.6913	0.6195	0.4923	0.3179	7.4644
		$N_l = 16$	0.6913	0.6195	0.4924	0.3179	7.4648
		$N_l = 32$	0.6913	0.6195	0.4924	0.3179	7.4649
		$N_l = 40$	0.6913	0.6195	0.4924	0.3179	7.4649
$\left[0^0/90^0/0^0/90^0\right]_s$	5	$(\hat{m},\ \hat{n})$	(1, 1)	(1, 1)	(1, 1)	(1, 1)	(1, 1)
		$N_l = 8$	0.6863	0.6139	0.4854	0.3070	7.4760
		$N_l = 16$	0.6863	0.6139	0.4854	0.3070	7.4768
		$N_l = 32$	0.6863	0.6139	0.4854	0.3070	7.4770
		$N_l = 40$	0.6863	0.6139	0.4854	0.3070	7.4770
$\left[0^0/90^0\right]_s$	10	$(\hat{m},\ \hat{n})$	(1, 2)	(1, 2)	(1, 2)	(1, 2)	(2, 2)
		$N_l = 4$	0.2737	0.2478	0.2030	0.1448	17.0609
		$N_l = 8$	0.2737	0.2478	0.2030	0.1448	17.0606
		$N_l = 16$	0.2737	0.2478	0.2030	0.1449	17.0606
		$N_l = 32$	0.2737	0.2478	0.2030	0.1449	17.0606
		$N_l = 40$	0.2737	0.2478	0.2030	0.1449	17.0606
$\left[0^0/90^0\right]_s$	20	$(\hat{m},\ \hat{n})$	(1, 2)	(1, 2)	(1, 2)	(1, 2)	(3, 3)
		$N_l = 4$	0.1079	0.0983	0.0818	0.0609	40.2368
		$N_l = 8$	0.1079	0.0983	0.0818	0.0609	40.2347
		$N_l = 16$	0.1079	0.0983	0.0818	0.0609	40.2342
		$N_l = 32$	0.1079	0.0983	0.0818	0.0609	40.2341
		$N_l = 40$	0.1079	0.0983	0.0818	0.0609	40.2341
$\left[0^0/90^0\right]_s$	100	$(\hat{m},\ \hat{n})$	(1, 4)	(1, 4)	(1, 4)	(1, 4)	(7, 7)
		$N_l = 4$	0.01300	0.01227	0.01108	0.00976	233.3586
		$N_l = 8$	0.01300	0.01227	0.01108	0.00976	233.3545
		$N_l = 16$	0.01300	0.01227	0.01108	0.00976	233.3534
		$N_l = 32$	0.01300	0.01227	0.01108	0.00976	233.3532
		$N_l = 40$	0.01300	0.01227	0.01108	0.00976	233.3531

in which $\Gamma^{(m)}(\zeta)$ (m=1-3) are given in Eq. (49), and ρ_0=2702 kg/m^3 (aluminum) and ρ_f=3800 kg/m^3 (alumina).

Table 6: The present modified Pagano solutions of the lowest frequency and critical load parameters of axially loaded and simply supported, laminated orthotropic cylinders with different values of the compressive load (L/R=5, $\bar{\omega} = \omega\ (10)\ \sqrt{\rho_f H^2/E_f}$) and $(\bar{P}_x)_{cr} = (P_x)_{cr} R^2/\left(2\pi R E_f H^3\right)$.

κ_p	R/H	Present	$\bar{\omega}$ $(P_x = 0)$	$\bar{\omega}$ $(P_x = 0.2\,(P_x)_{cr})$	$\bar{\omega}$ $(P_x = 0.5\,(P_x)_{cr})$	$\bar{\omega}$ $(P_x = 0.8\,(P_x)_{cr})$	$(\bar{P}_x)_{cr}$ (Pure stability)
0	5	$(\hat{m},\ \hat{n})$	(1, 2)	(1, 2)	(1, 2)	(1, 2)	(2, 2)
		$N_l = 10$	0.3824	0.3507	0.2968	0.2307	1.8415
		$N_l = 20$	0.3825	0.3507	0.2968	0.2307	1.8415
		$N_l = 40$	0.3825	0.3507	0.2968	0.2307	1.8415
		$N_l = 80$	0.3825	0.3507	0.2968	0.2307	1.8415
2	5	$(\hat{m},\ \hat{n})$	(1, 1)	(1, 1)	(1, 1)	(1, 1)	(2, 2)
		$N_l = 10$	0.3433	0.3132	0.2617	0.1971	1.3897
		$N_l = 20$	0.3440	0.3138	0.2621	0.1974	1.3898
		$N_l = 40$	0.3441	0.3139	0.2623	0.1975	1.3898
		$N_l = 80$	0.3442	0.3140	0.2623	0.1975	1.3898
∞	5	$(\hat{m},\ \hat{n})$	(1, 1)	(1, 1)	(1, 1)	(1, 1)	(2, 2)
		$N_l = 10$	0.3104	0.2817	0.2322	0.1688	1.1093
		$N_l = 20$	0.3104	0.2817	0.2322	0.1688	1.1093
		$N_l = 40$	0.3104	0.2817	0.2322	0.1688	1.1093
		$N_l = 80$	0.3104	0.2817	0.2322	0.1688	1.1093
2	10	$(\hat{m},\ \hat{n})$	(1, 2)	(1, 2)	(1, 2)	(1, 2)	(1, 2)
		$N_l = 10$	0.1132	0.1012	0.0800	0.0506	2.8839
		$N_l = 20$	0.1134	0.1015	0.0802	0.0507	2.8859
		$N_l = 40$	0.1135	0.1015	0.0802	0.0508	2.8864
		$N_l = 80$	0.1135	0.1015	0.0803	0.0508	2.8865
2	100	$(\hat{m},\ \hat{n})$	(1, 3)	(1, 3)	(1, 3)	(1, 3)	(1, 3)
		$N_l = 10$	0.004236	0.003789	0.002995	0.001895	40.4018
		$N_l = 20$	0.004245	0.003797	0.003002	0.001898	40.4203
		$N_l = 40$	0.004247	0.003799	0.003003	0.001899	40.4254
		$N_l = 80$	0.004248	0.003799	0.003004	0.001900	40.4266

Table 6 shows the solutions of the lowest frequency parameters of axially loaded and simply supported, FGM sandwich cylinders with different values of the compressive load, in which N_l=10, 20, 40 and 80; R/H=5, 10 and 100, L/R=5, and

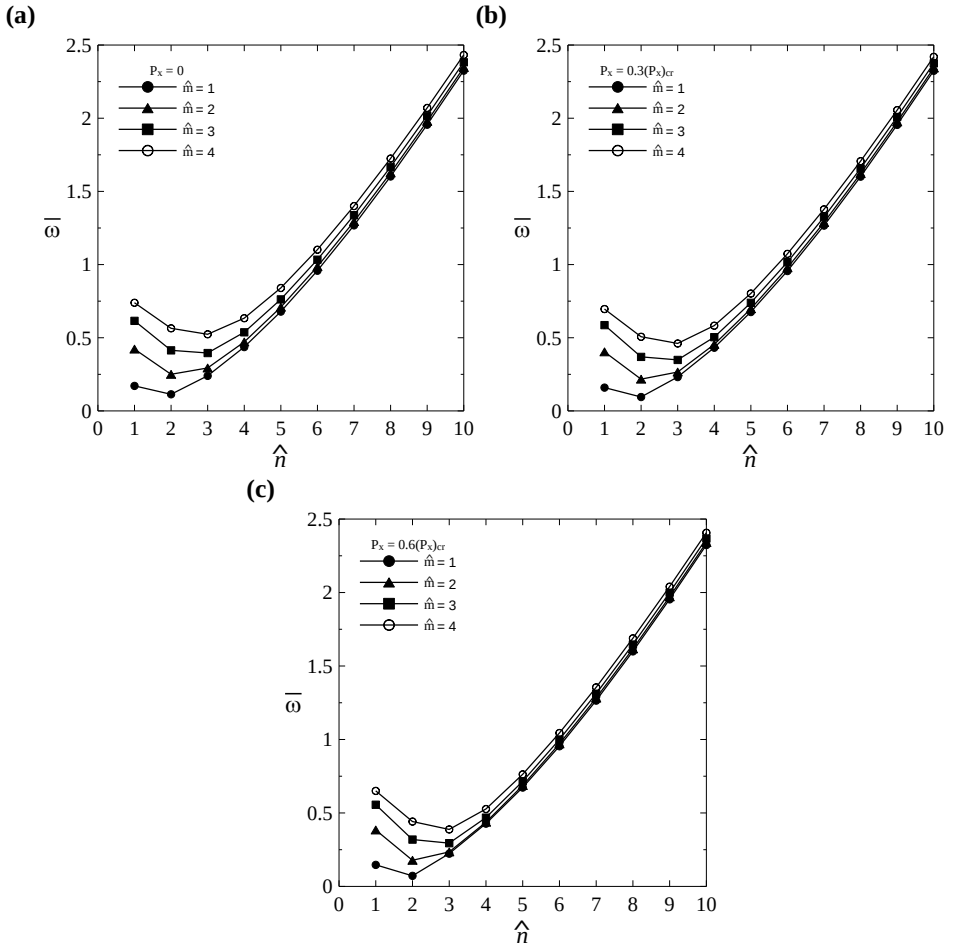

Figure 4: Variations of the lowest frequency parameters of axially loaded, FGM sandwich cylinders with the half-wave numbers $\hat{n}$ for $\hat{m}$=1-4 and $\kappa_p = 2$, (a) $P_x = 0$, (b) $P_x = 0.3\ (P_x)_{cr}$, (c) $P_x = 0.6\ (P_x)_{cr}$.

$h_1 : h_2 : h_3 = 0.2H : 0.6H : 0.2H$; P_x= 0, 0.2 $(P_x)_{cr}$, 0.5 $(P_x)_{cr}$ and 0.8 $(P_x)_{cr}$, and $(\bar{P}_x)_{cr} = (P_x)_{cr} R^2/(2\pi RH^3 E_f)$; κ_p=0, 2 and ∞. It can be seen in Table 6 that the convergence of the solutions is rapid. For example: in the case of a thick FGM sandwich cylinder, the relative error between the ten-layer solution and the eighty-layer one is less than 0.3%, and that between the twenty-layer solution and the eighty-layer one is less than 0.06%. The lowest frequency parameter decreases when the magnitude of the compressive load and the material-property gradient index become larger, which means the overall stiffness of the cylinder becomes

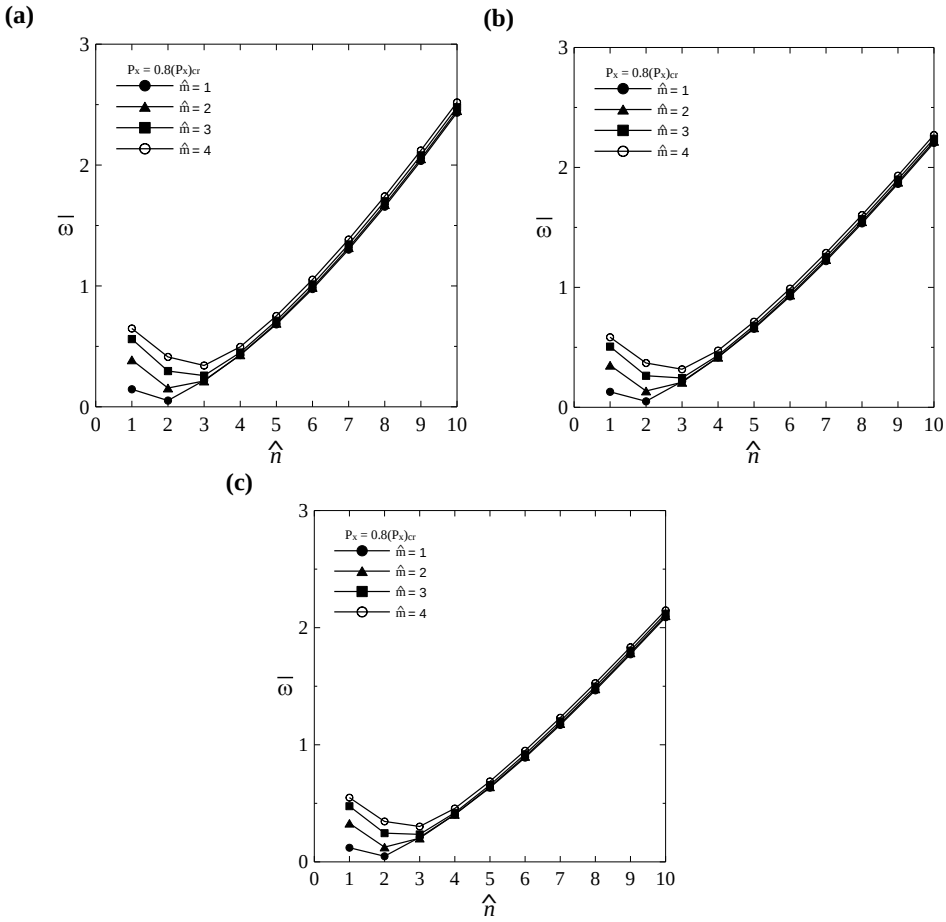

Figure 5: Variations of the lowest frequency parameters of axially loaded, FGM sandwich cylinders with the half-wave numbers $\hat{n}$ for $\hat{m}$=1-4 and $P_x = 0.8\,(P_x)_{cr}$, (a) $\kappa_p = 1$, (b) $\kappa_p = 5$, (c) $\kappa_p = 100$.

softer. It is also shown that the lowest critical load parameter of the cylinder decreases when the material-property gradient index becomes larger, and when the cylinder becomes thinner.

Figures 4 and 5 show the variations of the lowest frequency parameters of each vibration mode of the cylinders with different values of the applied compressive load and different material-property gradient indices, respectively, in which $\hat{m} = 1 - 4$ and $\hat{n} = 1 - 10$; R/H=10, L/R=5, and $h_1 : h_2 : h_3 = 0.2H : 0.6H : 0.2H$; P_x=0, 0.3 $(P_x)_{cr}$ and 0.6 $(P_x)_{cr}$, and $\kappa_p = 2$ in the former; $P_x = 0.8\,(P_x)_{cr}$, and κ_p=1, 5

and 100 in the latter. It is shown that when the value of $\hat{m}$ is fixed, the frequency parameter first decreases, and then it monotonically increases for all the cases considered, and the fundamental frequency parameters always occur at the vibration mode $(\hat{m},\ \hat{n}) = (1,\ 2)$, which means the fundamental vibration mode will not be affected by changing values of P_x and κ_p, while the corresponding frequency parameter is affected, and again it decreases when these become larger.

6 Concluding remarks

In this paper, we have developed a modified Pagano method for the exact 3D free vibration analyses of simply-supported, FGM sandwich cylinders and laminated composite ones, subjected to axial compression. The state space equations of this 3D problem were derived using the RMVT-based Hamilton principle, in which a pre-buckling state of 3D deformations was assumed. A set of initial normal stresses associated with these deformations was determined using a transfer matrix method combined with an SA one, and then it was introduced in the RMVT-based formulation. These state space equations can be reduced to the ones of pure free vibration and stability problems of the cylinders by letting the applied compressive load vanish for the former as well as discarding the inertia force terms and replacing all field variables with their incremental ones perturbed from the neutral equilibrium state for the latter. The accuracy and convergence of the solutions for the pure stability and pure free vibration of laminated composite cylinders were evaluated in comparison with the exact and approximate 3D solutions available in the open literature, with which the solutions were shown to converge rapidly and be in excellent agreement. A parametric study of the influences of the radius-to-thickness and length-to-radius ratios, thickness ratio for each layer, and material-property gradient index on the lowest frequency and critical load parameters of the FGM sandwich cylinders was undertaken. The results show that the effect of the initial transverse normal stress on the critical load parameters of the axially loaded cylinders is relatively minor, and can be neglected, and that von K'arm'an's nonlinearity assumption is not recommended for the stability analysis of thick cylinders. In addition, the solutions using a uniform initial strain and stress assumptions closely agree to each other; the fundamental vibration and critical buckling modes of FGM sandwich cylinders will not be affected with changing values of the material-property gradient index and core/face sheet thickness ratio, while the corresponding lowest frequency and critical load parameter decrease when these become larger. Furthermore, the present solutions may serve as benchmarks for assessing the accuracy and convergence of various approximate 2D theories of FGM sandwich cylinders, and they can also provide a reference for making suitable kinetic and kinematic assumptions prior to developing more advanced 2D theories of FGM cylinders.

Acknowledgement: This work was supported by the National Science Council of Taiwan, the Republic of China, through Grant NSC 100-2221-E-006-180-MY3.

Appendix A

The coefficients $\bar{k}_{ij}^{(m)}$ and $\bar{l}_{ij}^{(m)}$ in Eq. (37) are given by

$$\bar{k}_{14}^{(m)} = \left(\tilde{c}_{55}^{(m)}\right)^{-1}(h/R), \quad \bar{k}_{16}^{(m)} = -\tilde{m}, \quad \bar{k}_{22}^{(m)} = (\gamma_2)^{-1}(h/R),$$

$$\bar{k}_{25}^{(m)} = \left(\tilde{c}_{44}^{(m)}\right)^{-1}(h/R), \quad \bar{k}_{26}^{(m)} = \tilde{n}\,(\gamma_2)^{-1}, \quad \bar{k}_{31}^{(m)} = -\tilde{m}\,\tilde{Q}_{12}^{(m)}\,(\gamma_2)^{-1},$$

$$\bar{k}_{32}^{(m)} = \tilde{n}\,\tilde{Q}_{22}^{(m)}\,(\gamma_2)^{-2}, \quad \bar{k}_{33}^{(m)} = \left(Q_{23}^{(m)} - 1\right)(\gamma_2)^{-1}(h/R),$$

$$\bar{k}_{34}^{(m)} = \tilde{m}, \quad \bar{k}_{35}^{(m)} = -\tilde{n}\,(\gamma_2)^{-1}, \quad \bar{k}_{36}^{(m)} = \tilde{Q}_{22}^{(m)}\,(\gamma_2)^{-2},$$

$$\bar{k}_{41}^{(m)} = \tilde{m}^2\,\tilde{Q}_{11}^{(m)} + \tilde{n}^2\,\tilde{Q}_{66}^{(m)}\,(\gamma_2)^{-2}, \quad \bar{k}_{42}^{(m)} = -\tilde{m}\tilde{n}\left(\tilde{Q}_{12}^{(m)} + \tilde{Q}_{66}^{(m)}\right)(\gamma_2)^{-1},$$

$$\bar{k}_{43}^{(m)} = -\tilde{m}\,Q_{13}^{(m)}\,(h/R), \quad \bar{k}_{44}^{(m)} = -(\gamma_2)^{-1}\,(h/R),$$

$$\bar{k}_{46}^{(m)} = -\tilde{m}\,\tilde{Q}_{12}^{(m)}\,(\gamma_2)^{-1}, \quad \bar{k}_{51}^{(m)} = -\tilde{m}\tilde{n}\left(\tilde{Q}_{12}^{(m)} + \tilde{Q}_{66}^{(m)}\right)(\gamma_2)^{-1},$$

$$\bar{k}_{52}^{(m)} = \tilde{m}^2\tilde{Q}_{66}^{(m)} + \tilde{n}^2\,\tilde{Q}_{22}^{(m)}\,(\gamma_2)^{-2}, \quad \bar{k}_{53}^{(m)} = \tilde{n}\,Q_{23}^{(m)}\,(\gamma_2)^{-1}(h/R),$$

$$\bar{k}_{55}^{(m)} = -2\,(\gamma_2)^{-1}(h/R), \quad \bar{k}_{56}^{(m)} = \tilde{n}\,\tilde{Q}_{22}^{(m)}\,(\gamma_2)^{-2}, \quad \bar{k}_{61}^{(m)} = \tilde{m}\,Q_{13}^{(m)}\,(h/R),$$

$$\bar{k}_{62}^{(m)} = -\tilde{n}\,Q_{23}^{(m)}\,(\gamma_2)^{-1}(h/R), \quad \bar{k}_{63}^{(m)} = \left(\tilde{c}_{33}^{(m)}\right)^{-1}(h/R)^2,$$

$$\bar{k}_{66}^{(m)} = -Q_{23}^{(m)}\,(\gamma_2)^{-1}(h/R), \quad \bar{l}_{30}^{(m)} = \left(\tilde{c}_{33}^{(m)}\right)^{-1}\hat{f}_r^{(m)},$$

$$\bar{l}_{31}^{(m)} = -\tilde{m}\,Q_{13}^{(m)}\left(\hat{f}_r^{(m)},_3\right)(R/h) - \tilde{m}\,Q_{13}^{(m)}\,\hat{f}_r^{(m)}\,(\gamma_2)^{-1} + \tilde{m}\,Q_{13}^{(m)}\,Q_{23}^{(m)}\,\hat{f}_r^{(m)}\,(\gamma_2)^{-1},$$

$$\begin{aligned}\bar{l}_{32}^{(m)} =& 2\tilde{n}\,\hat{f}_\theta^{(m)}\,(\gamma_2)^{-2} + \tilde{n}\,Q_{23}^{(m)}\left(\hat{f}_r^{(m)},_3\right)(\gamma_2)^{-1}(R/h) + \tilde{n}\,Q_{23}^{(m)}\,\hat{f}_r^{(m)}\,(\gamma_2)^{-2} \\ & - \tilde{n}\,Q_{23}^{(m)}\,Q_{23}^{(m)}\,\hat{f}_r^{(m)}\,(\gamma_2)^{-2},\end{aligned}$$

$$\begin{aligned}\bar{l}_{33}^{(m)} =& -\left(\tilde{c}_{33}^{(m)}\right)^{-1}\left(\hat{f}_r^{(m)},_3\right) - \left(\tilde{c}_{33}^{(m)}\right)^{-1}\hat{f}_r^{(m)}\,(\gamma_2)^{-1}(h/R) \\ & + \left(\tilde{c}_{33}^{(m)}\right)^{-1} Q_{23}^{(m)}\,\hat{f}_r^{(m)}\,(\gamma_2)^{-1}(h/R),\end{aligned}$$

$$\bar{l}_{34}^{(m)} = -\tilde{m}\left(\tilde{c}_{55}^{(m)}\right)^{-1} Q_{13}^{(m)}\,\hat{f}_r^{(m)}, \quad \bar{l}_{35}^{(m)} = \tilde{n}\left(\tilde{c}_{44}^{(m)}\right)^{-1} Q_{23}^{(m)}\,\hat{f}_r^{(m)}\,(\gamma_2)^{-1},$$

$$\bar{l}_{36}^{(m)} = (\tilde{m})^2 \left(\hat{f}_x^{(m)} + Q_{13}^{(m)} \hat{f}_r^{(m)}\right)(R/h) + (\tilde{n})^2 \left(\hat{f}_\theta^{(m)} + Q_{23}^{(m)} \hat{f}_r^{(m)}\right)(\gamma_2)^{-2}(R/h) + \hat{f}_\theta^{(m)}(\gamma_2)^{-2} + Q_{23}^{(m)} \left(\hat{f}_r^{(m)},_3\right)(\gamma_2)^{-1}(R/h) - Q_{23}^{(m)} Q_{23}^{(m)} \hat{f}_r^{(m)}(\gamma_2)^{-2},$$

$$\bar{l}_{40}^{(m)} = \left(\tilde{c}_{55}^{(m)}\right)^{-1} \hat{f}_r^{(m)}, \quad \bar{l}_{41}^{(m)} = \tilde{m}^2 \hat{f}_x^{(m)} + \tilde{n}^2 \hat{f}_\theta^{(m)}(\gamma_2)^{-2} + \tilde{m}^2 Q_{13}^{(m)} \hat{f}_r^{(m)},$$

$$\bar{l}_{42}^{(m)} = -\tilde{m}\tilde{n} Q_{23}^{(m)} \hat{f}_r^{(m)}(\gamma_2)^{-1}, \quad \bar{l}_{43}^{(m)} = \tilde{m} \left(\tilde{c}_{33}^{(m)}\right)^{-1} \hat{f}_r^{(m)}(h/R),$$

$$\bar{l}_{44}^{(m)} = -\left(\tilde{c}_{55}^{(m)}\right)^{-1} \left(\hat{f}_r^{(m)},_3\right) - \left(\tilde{c}_{55}^{(m)}\right)^{-1} \hat{f}_r^{(m)}(\gamma_2)^{-1}(h/R),$$

$$\bar{l}_{46}^{(m)} = \tilde{m} \left(\hat{f}_r^{(m)},_3\right)(R/h) + \tilde{m} \hat{f}_r^{(m)}(\gamma_2)^{-1} - \tilde{m} Q_{23}^{(m)} \hat{f}_r^{(m)}(\gamma_2)^{-1},$$

$$\bar{l}_{50}^{(m)} = \left(\tilde{c}_{44}^{(m)}\right)^{-1} \hat{f}_r^{(m)}, \quad \bar{l}_{51}^{(m)} = -\tilde{m}\tilde{n} Q_{13}^{(m)} \hat{f}_r^{(m)}(\gamma_2)^{-1},$$

$$\bar{l}_{52}^{(m)} = \tilde{m}^2 \hat{f}_x^{(m)} + \tilde{n}^2 \hat{f}_\theta^{(m)}(\gamma_2)^{-2} + \hat{f}_\theta^{(m)}(\gamma_2)^{-2}(h/R) - \left(\hat{f}_r^{(m)},_3\right)(\gamma_2)^{-1} - \hat{f}_r^{(m)}(\gamma_2)^{-2}(h/R) + \tilde{n}^2 Q_{23}^{(m)} \hat{f}_r^{(m)}(\gamma_2)^{-2},$$

$$\bar{l}_{53}^{(m)} = -\tilde{n} \left(\tilde{c}_{33}^{(m)}\right)^{-1} \hat{f}_r^{(m)}(\gamma_2)^{-1}(h/R),$$

$$\bar{l}_{55}^{(m)} = -\left(\tilde{c}_{44}^{(m)}\right)^{-1} \left(\hat{f}_r^{(m)},_3\right) - 2\left(\tilde{c}_{44}^{(m)}\right)^{-1} \hat{f}_r^{(m)}(\gamma_2)^{-1}(h/R),$$

$$\bar{l}_{56}^{(m)} = 2\tilde{n} \hat{f}_\theta^{(m)}(\gamma_2)^{-2} - \tilde{n} \left(\hat{f}_r^{(m)},_3\right)(R/h) - \tilde{n} \hat{f}_r^{(m)}(\gamma_2)^{-2} + \tilde{n} Q_{23}^{(m)} \hat{f}_r^{(m)}(\gamma_2)^{-2}. \quad \text{(A1)}$$

The coefficients $\tilde{l}_{ij}^{(m)}$ in Eq. (38) are given by

$$\tilde{l}_{32}^{(m)} = 2\tilde{n} \hat{f}_\theta^{(m)}(\gamma_2)^{-2},$$

$$\tilde{l}_{36}^{(m)} = (\tilde{m})^2 \hat{f}_x^{(m)}(R/h) + (\tilde{n})^2 \hat{f}_\theta^{(m)}(\gamma_2)^{-2}(R/h) + \hat{f}_\theta^{(m)}(\gamma_2)^{-2},$$

$$\tilde{l}_{41}^{(m)} = \tilde{m}^2 \hat{f}_x^{(m)} + \tilde{n}^2 \hat{f}_\theta^{(m)}(\gamma_2)^{-2},$$

$$\tilde{l}_{52}^{(m)} = \tilde{m}^2 \hat{f}_x^{(m)} + \tilde{n}^2 \hat{f}_\theta^{(m)}(\gamma_2)^{-2} + \hat{f}_\theta^{(m)}(\gamma_2)^{-2}(h/R),$$

$$\tilde{l}_{56}^{(m)} = 2\tilde{n} \hat{f}_\theta^{(m)}(\gamma_2)^{-2}. \quad \text{(A2)}$$

The coefficients $\hat{l}_{ij}^{(m)}$ in Eq. (40) are given by

$$\hat{l}_{32}^{(m)} = \tilde{n} \hat{f}_\theta^{(m)}(\gamma_2)^{-2},$$

$$\widehat{l}_{36}^{(m)} = (\tilde{m})^2 \hat{f}_x^{(m)} (R/h) + (\tilde{n})^2 \hat{f}_\theta^{(m)} (\gamma_2)^{-2} (R/h) + \hat{f}_\theta^{(m)} (\gamma_2)^{-2},$$
$$\widehat{l}_{52}^{(m)} = \hat{f}_\theta^{(m)} (\gamma_2)^{-2} (h/R),$$
$$\widehat{l}_{56}^{(m)} = \tilde{n} \hat{f}_\theta^{(m)} (\gamma_2)^{-2}. \tag{A3}$$

The coefficients $\hat{l}_{ij}^{(m)}$ in Eq. (41) are given by

$$\hat{l}_{36}^{(m)} = (\tilde{m})^2 (R/h),$$
$$\hat{l}_{41}^{(m)} = \tilde{m}^2,$$
$$\hat{l}_{52}^{(m)} = \tilde{m}^2. \tag{A4}$$

Appendix B

The solution process of the transfer matrix method is described as follows:

According to Eq. (44), we obtain the general solution for the system equations of the m^{th}-layer ($m = 1, 2, \cdots, N_l$) in the form of

$$\mathbf{F}^{(m)}(x_3) = \Omega^{(m)}(x_3)\, \mathbf{L}^{(m)}. \tag{B1}$$

When $x_3 = x_{3(m-1)}$, in which $x_{3(m-1)} = \zeta_{m-1}/h$, according to Eq. (B1) we obtain

$$\mathbf{L}^{(m)} = \left[\Omega^{(m)}\left(x_{3(m-1)}\right)\right]^{-1} \mathbf{F}_{(m-1)}, \tag{B2}$$

where $x_{3(m-1)}$ is the dimensionless thickness coordinate measured from the middle surface to the bottom surface of m^{th}-layer, $\mathbf{F}_{(m-1)}$ denotes the vector of primary field variables at the interface between the $(m\text{-}1)^{th}$- and m^{th}-layers, and $\mathbf{F}_{(m-1)} = \mathbf{F}^{(m)}\left(x_3 = x_{3(m-1)}\right)$.

When $x_3 = x_{3(m)}$, in which $x_{3(m)} = \zeta_m/h$, using Eqs. (B1) and (B2), we obtain

$$\mathbf{F}_{(m)} = \mathbf{R}_{(m)}\, \mathbf{F}_{(m-1)}, \tag{B3}$$

where $\mathbf{R}_{(m)} = \Omega^{(m)}\left(x_{3(m)}\right)\left[\Omega^{(m)}\left(x_{3(m-1)}\right)\right]^{-1}$.

By analogy, the vectors of primary variables in the elastic and electric fields between the top and bottom surfaces of the cylinder (i.e., $\mathbf{F}_{(N)}$ and $\mathbf{F}_{(0)}$) are linked by

$$\mathbf{F}_{(N_l)} = \mathbf{R}_{(N_l)}\, \mathbf{F}_{(N_l-1)} = \left(\prod_{m=1}^{N_l} \mathbf{R}_{(m)}\right) \mathbf{F}_{(0)}, \tag{B4}$$

where $\prod_{m=1}^{N_l} \mathbf{R}_{(m)} = \mathbf{R}_{(N_l)} \mathbf{R}_{(N_l-1)} \cdots \mathbf{R}_{(2)} \mathbf{R}_{(1)}$.

Equation (B4) represents a set of six simultaneous algebraic equations. Imposing the boundary conditions prescribed on the lateral surfaces, we may rewrite the equation as

$$\begin{bmatrix} \mathbf{0} \\ \mathbf{F}_u \end{bmatrix} = \begin{bmatrix} \mathbf{R_{II}} & \mathbf{R_{III}} \\ \mathbf{R_{III}} & \mathbf{R_{IIII}} \end{bmatrix} \begin{bmatrix} \mathbf{0} \\ \mathbf{F}_b \end{bmatrix}, \tag{B5}$$

where $\mathbf{F}_u$ and $\mathbf{F}_b$ denote the unknown variables on the outer and inner surfaces, respectively.

According to Eq. (B5), we have a set of homogeneous equations as

$$\mathbf{R_{I\,II}}\, \mathbf{F}_b = \mathbf{0}, \tag{B6}$$

where $\mathbf{R_{I\,II}}$ is a 3x3 matrix, in which the coefficients are related to the dimensionless applied load ($\bar{p}_x$) and natural frequency (ω_τ).

A nontrivial solution of Eq. (B6) exists if the determinant of the coefficient matrix vanishes. The natural frequencies of FGPM sandwich cylinders for a set of fixed values ($\hat{m}$, $\hat{n}$) can be obtained by

$$R\,(\bar{p}_x,\ \omega_\tau) = |\mathbf{R_{III}}| = 0. \tag{B7}$$

Equation (B7) is called the characteristic equation. Since the determinant of $\mathbf{R_{I\,II}}$ yields an implicit function of $\bar{p}_x$ and ω_τ rather than an explicit one, a bisection method is used to determine the roots of Eq. (B7).

References

Carrera, E. (2003): Theories and finite elements for multilayered plates and shells: A unified compact formulation with numerical assessment and benchmarks. *Archives of Computational Methods in Engineering*, vol. 10, pp. 215-296.

Chen, C. S. (2005): Investigation on the vibration and stability of hybrid composite plates. *Journal of Reinforced Plastics and Composites*, vol. 24, pp. 1747-1758.

Chen, C. S.; Fung, C. P.; Chien, R. D. (2006): Analysis of an initially stresses hybrid plate based on a higher-order theory. *Composite Structures*, vol. 74, pp. 343-353.

Chen, C. S.; Fung, C. P.; Yu, S. Y. (2008): The investigation on the vibration and stability of functionally graded plates. *Journal of Reinforced Plastics and Composites*, vol. 27, pp. 1435-1447.

Chen, C. S.; Hsu, C. Y.; Tzou, G. J. (2009): Vibration and stability of functionally graded plates based on a higher-order deformation theory. *Journal of Reinforced Plastics and Composites*, vol. 28, pp. 1215-1234.

Chen, W. Q.; Ding, H. J. (2002): On free vibration of a functionally graded piezoelectric rectangular plate. *Acta Mechanica*, vol. 153, pp. 207-216.

Chen, W. Q.; Wang, L. Z. (2002): Free vibrations of functionally graded piezoceramic hollow spheres with radial polarization. *Journal of Sound and Vibration*, vol. 251, pp. 103-114.

Chen, W. Q.; Bian, Z. G.; Lv, C. F.; Ding, H. J. (2004): 3D free vibration analysis of a functionally graded piezoelectric hollow cylinder filled with compressible fluid. *International Journal of Solids and Structures*, vol. 41, pp. 947-964.

Dong, L.; Atluri, S. N. (2011): A simple procedure to develop efficient & stable hybrid/mixed elements, and Voronoi cell finite elements for macro- & micromechanics. *CMC-Computers, Materials, & Continua*, vol. 24, pp. 61-104.

Dong, L.; El-Gizawy, A. S., Juhany, K. A.; Atluri, S. N. (2014): A simple locking-alleviated 4-node mixed-collocation finite element with over-integration, for homogeneous or functionally-graded or thick-section laminated composite beams. *CMC-Computers, Materials, & Continua*, vol. 40, pp. 49-77.

D'ottavio, M.; Carrera, E. (2010): Variable-kinematics approach for linearized buckling analysis of laminated plates and shells. *AIAA Journal*, vol. 48, pp. 1987-1996.

Matsunaga, H. (2007): Vibration and stability of cross-ply laminated composite shallow shells subjected to in-plane stresses. *Composite Structures*, vol. 78, pp. 377-391.

Matsunaga, H. (2008): Free vibration and stability of functionally graded shallow shells according to a 2D higher-order deformation theory. *Composite Structures*, vol. 84, pp. 132-146.

Matsunaga, H. (2009): Free vibration and stability of functionally graded circular cylindrical shells according to a 2D higher-order deformation theory. *Composite Structures*, vol. 88, pp. 519-531.

Najafov, A. M.; Sofiyev, A. H.; Kuruoglu, N. (2013): Torsional vibration and stability of functionally graded orthotropic cylindrical shells on elastic foundations. *Meccanica*, vol. 48, pp. 829-840.

Noor, A. K.; Rarig, P. L. (1974): Three-dimensional solutions of laminated cylinders. *Computer Methods in Applied Mechanics and Engineering*, vol. 3, pp. 319-334.

Pagano, N. J. (1969): Exact solutions for composite laminates in cylindrical bend-

ing. *Journal of Composite Materials*, vol. 3, pp. 398–411.

Pagano, N. J. (1970): Exact solutions for rectangular bidirectional composites and sandwich plates. *Journal of Composite Materials*, vol. 4, pp. 20–34.

Reissner, E. (1984): On a certain mixed variational theory and a proposed application. *International Journal for Numerical Methods in Eng*ineering, vol. 20, pp. 1366-1368.

Reissner, E. (1986): On a mixed variational theorem and on a shear deformable plate theory. *International Journal for Numerical Methods in Eng*ineering, vol. 23, pp. 193-198.

Sheng, G. G.; Wang, X. (2008): Thermal vibration, buckling and dynamic stability of functionally graded cylindrical shells embedded in an elastic medium. *Journal of Reinforced Plastics and Composites*, vol. 27, pp. 117-134.

Sheng, G. G.; Wang, X. (2010): Thermoelastic vibration and buckling analysis of functionally graded piezoelectric cylindrical shells. *Applied Mathematical Modelling*, vol. 34, pp. 2630-2643.

Soldatos, K. P.; Ye, J. Q. (1994): Three-dimensional static, dynamic, thermoelastic and buckling analysis of homogeneous and laminated composite cylinders. *Composite Structures,* vol. 29, vol. 131-143.

Wu, C. P.; Chen, S. J.; Chiu, K. H. (2010): Three-dimensional static behavior of functionally graded magneto-electro-elastic plates using the modified Pagano method. *Mechanics Research Communications*, vol. 37, pp. 54-60.

Wu, C. P.; Chiu, K. H.; Wang, Y. M. (2008): A review on the three-dimensional analytical approaches of multilayered and functionally graded piezoelectric plates and shells. *CMC: Computers, Materials, & Continua*, vol. 8, pp. 93-132.

Wu, C. P.; Jiang, R. Y. (2011): The 3D coupled analysis of FGPM circular hollow sandwich cylinders under thermal loads. *Journal of Intelligent Material Systems and Structures*, vol. 22, pp. 691-712.

Wu, C. P.; Liu, K. Y. (2007): A state space approach for the analysis of doubly curved functionally graded elastic and piezoelectric shells. *CMC-Computers, Materials, & Continua*, vol. 6, pp. 177-199.

Wu, C. P.; Lu, Y. C. (2009): A modified Pagano method for the 3D dynamic responses of functionally graded magneto-electro-elastic plates. *Compositer Struct*ures, vol. 90, pp. 363-372.

Wu, C. P.; Syu, Y. S. (2007): Exact solutions of functionally graded piezoelectric shells under cylindrical bending. *International Journal of Solids and Structures*, vol. 44, pp. 6450-6472.

Wu, C. P.; Tsai, Y. H. (2004): Asymptotic DQ solutions of functionally graded

annular spherical shells. *European Journal of Mechanics A-Solids*, vol. 23, pp. 283-299.

Wu, C. P.; Tsai, Y. H. (2009): Cylindrical bending vibration of functionally graded piezoelectric shells using the method of perturbation. *Journal of Engineering Mathematics*, vol. 63, pp. 95-119.

Wu, C. P.; Tsai, Y. H. (2010): Dynamic responses of functionally graded magneto-electro-elastic shells with closed-circuit surface conditions using the method of multiple scales. *European Journal of Mechanics A-Solids*, vol. 29, pp. 166-181.

Wu, C. P.; Tsai, T. C. (2011): Exact solutions of functionally graded piezoelectric material sandwich cylinders by a modified Pagano method. *Applied Mathematical Modelling*, vol. 36, pp. 1910-1930.

Wu, C. P.; Yang, S. W. (2011): RMVT-based meshless collocation and element-free Galerkin methods for the approximate 3D analysis of multilayered composite and FGM circular hollow cylinders. *Composites Part B-Engineering*, vol. 42, pp. 1683-1700.

Ye, J.; Soldatos, K. P. (1995): Three-dimensional buckling analysis of laminated composite hollow cylinders and cylindrical panels. *International Journal of Solids and Structures*, vol. 32, pp. 1949-1962.